APPLIED PHYSICS REVIEWS

Nanoscale thermal transport

David G. Cahill[a)]
Department of Material Science and Engineering and the Frederick Seitz Materials Research Laboratory, University of Illinois, Urbana, Illinois 61801

Wayne K. Ford
Intel Corporation, 5200 NE Elam Young Parkway, Hillsboro, Orgeon 97124

Kenneth E. Goodson
Department of Mechanical Engineering, Stanford University, Palo Alto, California 94305

Gerald D. Mahan
Department of Physics, Pennsylvania State University, University Park, Pennsylvania 16802

Arun Majumdar
Department of Mechanical Engineering, University of California, Berkeley, California 94720

Humphrey J. Maris
Department of Physics, Brown University, Providence, Rhode Island 02912

Roberto Merlin
Department of Physics, University of Michigan, Ann Arbor, Michigan 48109

Simon R. Phillpot
Materials Science Division, Argonne National Laboratory, Argonne, Illinois 60439

(Received 28 January 2002; accepted 1 August 2002)

Rapid progress in the synthesis and processing of materials with structure on nanometer length scales has created a demand for greater scientific understanding of thermal transport in nanoscale devices, individual nanostructures, and nanostructured materials. This review emphasizes developments in experiment, theory, and computation that have occurred in the past ten years and summarizes the present status of the field. Interfaces between materials become increasingly important on small length scales. The thermal conductance of many solid–solid interfaces have been studied experimentally but the range of observed interface properties is much smaller than predicted by simple theory. Classical molecular dynamics simulations are emerging as a powerful tool for calculations of thermal conductance and phonon scattering, and may provide for a lively interplay of experiment and theory in the near term. Fundamental issues remain concerning the correct definitions of temperature in nonequilibrium nanoscale systems. Modern Si microelectronics are now firmly in the nanoscale regime—experiments have demonstrated that the close proximity of interfaces and the extremely small volume of heat dissipation strongly modifies thermal transport, thereby aggravating problems of thermal management. Microelectronic devices are too large to yield to atomic-level simulation in the foreseeable future and, therefore, calculations of thermal transport must rely on solutions of the Boltzmann transport equation; microscopic phonon scattering rates needed for predictive models are, even for Si, poorly known. Low-dimensional nanostructures, such as carbon nanotubes, are predicted to have novel transport properties; the first quantitative experiments of the thermal conductivity of nanotubes have recently been achieved using microfabricated measurement systems. Nanoscale porosity decreases the permittivity of amorphous dielectrics but porosity also strongly decreases the thermal conductivity. The promise of improved thermoelectric materials and problems of thermal management of optoelectronic devices have stimulated extensive studies of semiconductor superlattices; agreement between experiment and theory is generally poor. Advances in measurement methods, e.g., the 3ω method, time-domain thermoreflectance, sources of coherent phonons, microfabricated test structures, and the scanning thermal microscope, are enabling new capabilities for nanoscale thermal metrology. © *2003 American Institute of Physics.* [DOI: 10.1063/1.1524305]

[a)]Electronic mail: d-cahill@uiuc.edu

TABLE OF CONTENTS

I. INTRODUCTION

Recent advances in synthesis, processing, and microanalysis are enabling the routine production of well-characterized materials with structure that varies on the length scale of several nanometers. Examples are semiconductor quantum dots and superlattices, polymer nanocomposites, multilayer coatings, microelectronic and optoelectronic devices, and microelectromechanical sensors. Many of these nanoscale structures already have important commercial applications, while others are studied scientifically. The most important devices, in terms of worldwide sales, are the integrated circuits used in computer circuits and memories. Device engineers have been astonishingly clever at maintaining Moore's Law, which states that the individual device components get smaller every year. Soon the field-effect-transistors (FET) will have a channel length of 100 nm, and 50 nm devices are projected in the near future. In most current and envisioned applications of nanostructures, thermal management is a serious issue. In some devices, such as computer processors or semiconductor lasers, one wants to get the heat away as efficiently as possible—these systems need high thermal conductivity. In others, such as thermal barriers or thermoelectric materials used for solid-state refrigeration, one wants the thermal conductivity to be as small as possible.

Our discussion emphasizes thermal transport in nonmetallic systems, in which heat is transported by phonons. Phonons have a wide variation in frequency, and an even larger variation in their mean-free-paths (mfps). However, the bulk of the heat is often carried by phonons of large wave vector, and they have mfps at room temperature of 1–100 nm. So in many systems of current interest, the scale of the microstructure is the same scale as the mfp of the phonons, and sometimes comparable to the phonon wavelength. This clearly necessitates an understanding of heat transport beyond that achievable at the continuum level. So far, no analytical theories have adequately treated the wave nature of phonons that will be manifest at these length scales. Moreover, this equality in length scales raises important conceptual questions, among which is how to define temperature on the length scale of the phonon wavelength and phonon mfp.

This review will summarize the present understanding of thermal transport in nanostructures. The experimental difficulties begin with the severely limited capabilities for measuring thermal transport in increasingly small systems. A recent review summarizes the experimental techniques that are being used to probe thermal conduction at a submicron level.[1] These methods are also discussed here. Currently, the only method with nanometer-scale spatial resolution that may be applied to nanometer structures is based on the atomic force microscope (AFM). However, AFM measurements are only beginning to provide an understanding of thermal transport in nanoscale structures; the experimental field is certainly in its infancy.

The theory and simulation of nanoscale thermal transport is at a similarly immature stage. The recognition that a more detailed theoretical understanding of heat transport than achievable using Fourier's Law of heat conduction, $\dot{Q} = -\kappa \nabla T$ where $\dot{Q}$ is the heat flux, κ the thermal conductivity and ∇T the temperature gradient, has lead to the development of approaches based on the numerical solutions of the Boltzmann transport equation (BTE) and to atomic-level simulations of thermal conductivity. Each still requires further methodological developments and the first systematic applications of these methods to heat transport issues are still being refined.

Since interfaces play a critical role in nanoscale thermal transport, we begin our discussion with a review of experiments and theory on the transport of heat between two different materials or between twin or twist boundaries of the same material. In Sec. III, we focus on thermal transport in microfabricated nanostructures and synthetic nanostructures of reduced dimension. The related topic of heat transport in nanostructured thin film materials, including superlattices, is addressed in Sec. IV. We explore issues associated with metrology and measurement science in Sec. V.

II. HEAT TRANSPORT AND PHONON DYNAMICS AT INDIVIDUAL INTERFACES

The idea that an interface should produce a thermal resistance is intuitively appealing, since an interface constitutes an interruption in the regular crystalline lattice on which phonons propagate. For an interface between dissimilar materials, the different densities and sound speeds result in a mismatch in the acoustic impedances; this is directly analogous to the mismatch in the refractive indices of two optically different materials. The effect that this impedance mismatch has on phonon transmission is captured in the acoustic-mismatch (AM) model. By assuming that no scattering takes place at the interface, and by imposing appropriate stress and displacement boundary conditions at the interface, the AM model gives the transmission coefficient t_{AB} for phonon energy in material A incident normal to the interface with material B as:

$$t_{AB}=\frac{4Z_AZ_B}{(Z_A+Z_B)^2}, \tag{1}$$

where $Z=\rho c$ is the acoustic impedance, with c and ρ being the speed of sound and mass density, respectively.[2,3] In the AM model, the interface has no intrinsic properties but merely joins the two grains. As a consequence a twist grain boundary, in which the normals on the two sides of the GB are crystallographically identical, would incorrectly be predicted to have a transmission coefficient of one.

By contrast, in the diffuse mismatch (DM) model it is assumed that all phonons striking an interface loses memory of where they came from. Then, the probability of being scattered to one side of the interface or the other is simply proportional to the phonon density of states. Thus, as in the AM model, the fraction of energy transmitted is independent of the structure of the interface itself.[3]

While the above two models provide useful reference calculations against which to compare experimental results, and for many cases give rather similar predictions, neither captures the complexity of the interaction between phonons and real interfaces.

As we will see in this section, the interactions of phonons with a single interface still offers significant challenges to both experiments and theory/simulation. We first review experiments on thermal transport across individual interfaces, including both the classic Kapitza problem of a superfluid-helium/solid interface and model solid/solid interfaces. We point out that spectral methods, involving phonons of well-defined frequencies and wave vectors, offer the promise of providing insights into thermal transport not accessible to more traditional experiments. We summarize recent atomic-level simulations of thermal conductivity through individual interfaces and identify a need for simulations of the interaction of individual phonons with interfaces. Finally, we point out that the simulations of thermal conductivity raise fundamental thermodynamics issues concerning the definition of temperature of nonequilibrium nanoscale systems.

A. Thermal conductance of model interfaces

We consider the thermal conductance of an isolated interface, i.e., an interface that is separated from other interfaces by a distance that is large compared to the mean-free-path of the lattice vibrations that dominate heat transport in the material. In this limit, we can ignore coherent superposition of lattice waves reflected or transmitted by adjacent interfaces. Swartz and Pohl[3] give an exhaustive review of thermal boundary resistance, the inverse of interface thermal conductance, through 1988.

The existence of a thermal boundary resistance between a solid and superfluid helium was first detected by Kapitza in Ref. 4. When the discovery was first made, it was thought that this resistance was due to some special property of superfluid helium. Only later was it realized that such a Kaptiza resistance, R_K, exists at the interface between any pair of dissimilar materials. Khalatnikov[2] developed the acoustic-mismatch model to explain this thermal resistance. The acoustic mismatch is extremely large at an interface between helium and most ordinary solids because the density and sound velocity of helium are very much less than for other materials. While Khalatnikov's theory was able to explain the existence of the Kapitza resistance, the value of R_K that was calculated was between 10 and 100 times larger than typical experimental values measured at 1–2 K. This indicates that phonons are able to cross the interface substantially more easily than expected.

Remarkably, the reason for this so-called ''anomalous transmission'' at these low temperatures has still not been established. It was proposed by Challis, Dransfeld, and Wilks[5] that the transmission was increased due to the existence of a compressed layer of helium on the surface of the solid. This layer is formed because of the van der Waals attraction of helium atoms to a solid surface. An important experiment was performed by Weber *et al.*[6] They measured the transmission of phonons across the interface between an alkali–halide crystal and helium. Very clean surfaces were produced by cleaving the alkali-halide crystals at low temperature. For these surfaces no anomalous transmission was observed, indicating that the excess transmission must be associated with some sort of surface contamination or defects. Olson and Pohl[7] verified that the anomalous transmission between Si and liquid helium directly correlates with an increase in the diffuse phonon scattering.

Since the work of Weber *et al.*,[6] a number of attempts have been made to explain how surface contamination can have such a large effect on the transmission. Much of this work is reviewed in Refs. 3, 8, and 9. Despite these efforts, no generally accepted theory has emerged. The resolution of this problem requires more detailed experimental work under controlled conditions with well-characterized surfaces prepared and studied under ultrahigh vacuum.

Of course, while not directly relevant to technical problems of thermal management in nanostructures, the work on superfluid helium does leave open the possibility that the transmission of phonons across the interface between two solids may be substantially affected by a small number of

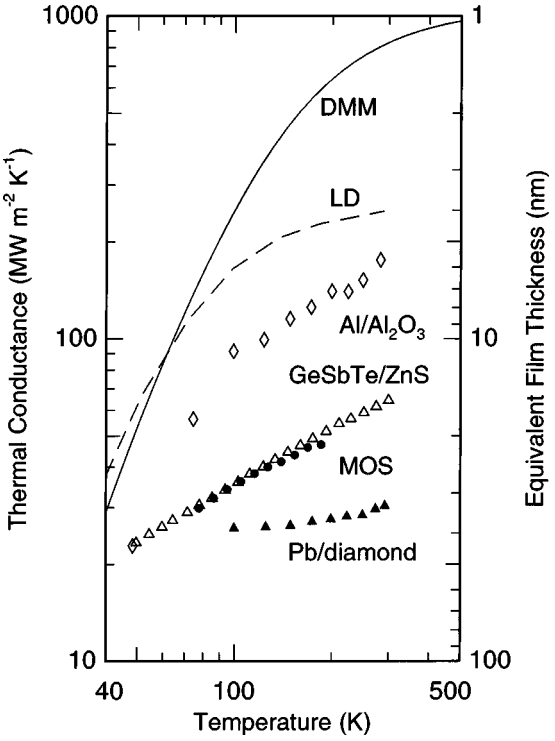

FIG. 1. Comparison of selected data for interface thermal conductance: (i) individual interfaces measured by picosecond thermoreflectance (Ref. 10), Al/Al_2O_3 (open diamonds) and Pb/*c*-C (filled triangles); (ii) conductance of the *a*-$GeSbTe_{2.5}$/ZnS interface (open triangles) from a multilayer sample (Ref. 14), (iii) series conductance of the top and bottom interfaces of metal–SiO_2–silicon structures (filled circles labeled by MOS) (Refs. 12 and 13). The solid line is the calculated diffuse mismatch conductance of Al/Al_2O_3 using the Debye model; the dashed line is the theoretical prediction for Al/Al_2O_3 using a lattice-dynamical calculation of a model fcc interface (Ref. 10). The right axis gives the thickness of a film with $\Lambda = 1\ W\ m^{-1}\ K^{-1}$ that has the thermal conductance corresponding to the left axis.

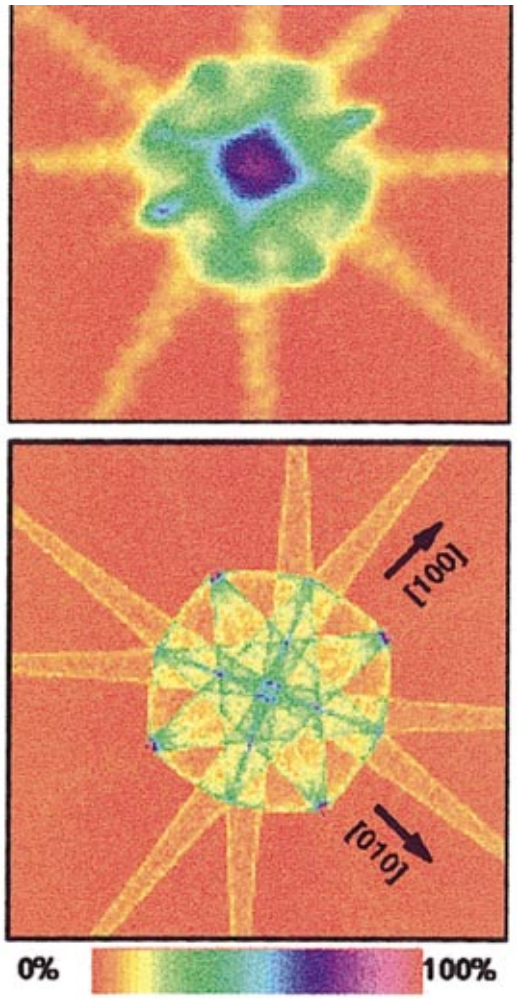

FIG. 2. (Color) Top: experimentally observed phonon focusing image in twist-bonded Si with a twist angle of 40 degrees (Ref. 17). Each of the two bonded crystals are 3 mm thick, the width of the image corresponds to 2 mm. Bottom: simulated image. Arrows indicate the crystal orientation relative to the phonon source. Phonon intensities are normalized to the maximum value in each image.

surface defects. The extent to which this occurs has not yet been established.

Some recent data for the thermal conductances of model solid/solid interfaces are shown in Fig. 1. Surprisingly, near room temperature, the highest thermal conductance for metal/dielectric interfaces measured by picosecond thermoreflectance,[10] Ti/Al_2O_3 and Al/Al_2O_3, is only a factor of ~ 5 larger than the lowest conductance, Pb/diamond. Other data for metal/dielectric interfaces,[3,11–13] for the most part, fall between these two extremes.

B. Heat pulse and coherent phonon experiments

Phonon transmission across a single interface has been studied using both coherent and incoherent phonons. To study incoherent phonons a pulse of energy is deposited into the material on one side of the interface. This generates incoherent phonons with a frequency spectrum that is determined by the pulse energy and the ambient temperature. These phonons propagate across the interface and are then detected in the material on the other side. This type of experiment has been performed for interfaces between solids and liquid helium (see, for example, Wichert *et al.*[15]) and at solid-solid interfaces (for a review, see Ref. 16). Usually, the experiments are performed at low temperatures so that the phonon mean free path is long; i.e., the phonons travel ballistically in the two media. As a result, it is possible to study separately the transmission of phonons of different polarization and to observe the refraction that occurs when the phonons cross the interface. This refraction, combined with the effects of phonon focusing lead to an interesting angular variation of the phonon flux emerging from the interface.[16] As an example, in Fig. 2 we show the phonon flux emerging from the interface between two twist-bonded Si crystals.[17] The faces of these crystals both have a (100) orientation, but one crystal is rotated by 40° around the [100] axis relative to the other.

To study the propagation of coherent phonons across an interface, the picosecond ultrasonic technique can be used. A short light pulse is absorbed in a material, and because of thermal expansion a short strain pulse (coherent phonon) is generated. This strain pulse is detected after it has been reflected or transmitted across the interface to another material. In this way the transmission of phonons of frequency up to

about 1 THz can be studied. In one experiment of this type, coherent phonon transmission at a bonded interface between SiO_2 and Si was studied.[18,19] It was possible to use the acoustic transmission as a measure of the quality of the bond, and to see how the bonding improved with thermal annealing. In another experiment,[20] a graded interface between films of gold and aluminum was studied. The interface width ζ was ~ 400 Å. For a diffuse interface the phonon transmission is expected to depend on the value of $k\zeta$, where k is the phonon wave number. For $k\zeta \geqslant 1$, the transmission should be larger because the acoustic properties vary smoothly on the scale of the phonon wavelength. The experiment demonstrated this effect.

Quantitative measurements with coherent phonons have many potential applications for the characterization of interfaces. In picosecond ultrasonics, the light creates sound pulses, i.e., a continuum of modes for which the relevant length scale is defined by the penetration depth of the light and other parameters of the overlayer. Periodic layered media offer an alternative method for generating coherent phonons. Here, phase-matching considerations show that light can couple to modes of wave vectors $q \approx 2\pi n/d$ where n is an integer and d is the period of the structure. Using femtosecond laser sources, this approach has been extensively applied to GaAs-$Al_xGa_{1-x}As$ (Ref. 21) and $In_xGa_{1-x}N$–GaN (Refs. 22 and 23) superlattices to generate coherent acoustic modes of frequencies up to ~ 1 THz.

C. Molecular-dynamics simulation of heat transport and phonon dynamics

Computational approaches to heat-transfer problems span the range from numerical solutions of Fourier's law[24] to calculations based on the Boltzmann transport equation (BTE)[25,26] to atomic-level simulations. In the Fourier and BTE approaches, the physics of heat transfer and phonon scattering are incorporated into the calculations in an explicit manner; thus for a reliable calculation, a fairly sophisticated understanding of the fundamental phonon processes is required. While in some cases (e.g., anharmonic phonon effects, isotopic defects, and point defects) understanding is well-developed, in others (e.g., interfaces) current understanding is poor. Molecular-dynamics (MD) simulation, by contrast, merely involves the integration in time of Newton's equations of motion for an ensemble of atoms interacting with each other through a, usually empirical, interatomic potential.[27,28] Because the formalism of the MD approach does not require any *a priori* understanding of heat transport, it is ideal for investigating the fundamental heat-transfer mechanisms themselves. However, MD does have the significant limitation of being entirely classical, with each vibrational mode equally excited; thus it is only rigorously applicable to solids above the Debye temperature. Moreover, since electrons are not included in an atomistic model, it is not possible to simulate electrical conductors or the electron–phonon interactions present in many semiconductors. In this subsection we briefly review recent atomic-level simulations of thermal transport at interfaces, and point out the opportunities for gaining important new insights from the simulation of individual phonon processes.

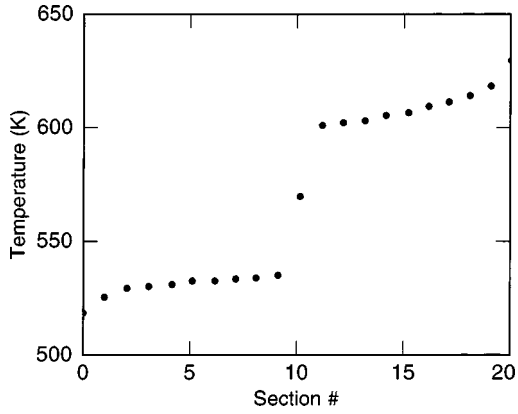

FIG. 3. Thermal profile calculated by MD for a $\Sigma = 13$ twin boundary in Si, after Ref. 31. The sample is 25 nm along the x axis and contains 840 atoms. Total simulation time is 1 ns.

The two most commonly used approaches to the MD simulation of the thermal conductivity are the Green–Kubo approach in which the equilibrium fluctuations in the heat current are analyzed, and the ''direct method,'' which mimics experiment by imposing a temperature gradient on the system and determining the thermal conductivity from Fourier's Law (for a recent review of these methods see Ref. 29). While simple in principle, in practice each has significant complications associated with system-size effects and the relatively long simulation times required. Moreover, the direct method has the additional complication of a potential nonlinear response of the system associated with the very large temperature gradients imposed (typically in excess of 10^9 K m^{-1}). A recent systematic comparison has shown that, when extrapolated to infinite system size, the Green–Kubo and direct methods give consistent values for the thermal conductivity, albeit each with error bars of 20% or more.[29] Despite the additional complications, it was concluded that the direct method is usually preferable, particularly when applied to interfacial systems, as it has the significant advantage of providing a direct measure of the interfacial resistance, R_K, from the temperature drop across the interface. (Unfortunately, however, as discussed in the next subsection, the conceptual issues associated with defining the temperature in an inhomogeneous system have yet to be fully resolved.)

There have been relatively few atomic-level simulations of heat transport at solid–solid interfaces. Pickett *et al.*[30] explored the transmission of phonon energy at an interface between two diamond-structured materials differing only in their masses. Maiti *et al.*[31] used the direct method to perform the first simulations of thermal transport through grain boundaries. Figure 3 shows the temperature profile through the simulation cell. The thermal conductance, G_K, of the interface can be calculated from the temperature drop ΔT, determined from the figure, and from the heat-current density $\dot{Q}$ passing through the system, determined from the simulation: $G_K = \dot{Q}/\Delta T$. For two different symmetric tilt grain boundaries in Si, they obtained $G_K = 0.8$ and $G_K = 0.9$ GW m^{-2} K^{-1}.

Recently, Schelling *et al.*[32] determined the thermal conductance for the (111) $\Sigma 31$ twist GB, which has a rather low energy, and for the (100) $\Sigma 29$ twist GB, which has a rather high energy, for the same interatomic description of Si and obtained values of 1.53 and 0.85 $\mathrm{GW\,m^{-2}\,K^{-1}}$, respectively. In a number of studies of the GBs in Si, Keblinski *et al.*[33] showed that the (100) $\Sigma 29$ GB is, from a structural point of view, representative of the many high-energy GBs in Si. Together with the very similar values for the two tilt GBs, this suggests that $G_K \approx 0.8-0.9\ \mathrm{GW\,m^{-2}\,K^{-1}}$ may be taken as representative of most GBs in Si. The much higher value for conductance of the (111) $\Sigma 31$ is reasonable given that the GBs on (111) plane have the lowest energy of all the high-angle GBs in Si.[33] In comparison with the experimental results show in Fig. 1, these values for the conductance are rather high. One possible reason for this is that all of the experimental systems are interfaces between dissimilar materials which, due to the acoustic-impedance mismatch, can be expected to have a lower conductance than a grain boundary. A second possible reason could be that the simulated grain boundaries are defect-free and atomically flat, thus presumably minimizing the thermal resistance.

It is useful to analyze the thermal resistance of an interface in terms of the length of perfect crystal that would provide an equivalent thermal resistance. This led Nan *et al.*[34] to define the Kapitza length, $l_K = \kappa / G_K$; typical values for Si ($\kappa \sim 100\ \mathrm{W\,m^{-1}\,K^{-1}}$ and $G_K \approx 1\ \mathrm{GW\,m^{-2}\,K^{-1}}$) give $l_K \sim 100$ nm as the thickness of perfect crystal with the same thermal resistance as the interface.

Figure 3 shows regions of nonlinear temperature change far from the GB. These nonlinear regions are close to the heat source and heat sink in the system and arise from the interface between the regions that are heated and cooled and the rest of the system. The interpretation of these nonlinear regions can draw from the results of phonon transport theory,[25,26] which has connections to the kinetic theory of molecular transport[35,36] and the equation of photon radiative transfer.[37,38] These increased temperature gradients resemble those predicted by the Boltzmann transport equations for gases, photons, and phonons.

Isothermal boundary conditions enforce perfect emission and absorption of phonons from the boundary, i.e., a phonon blackbody, and ensure equilibrium conditions for the emitted phonons. This has an influence comparable to an ensured phonon scattering event at the boundary. Phonons traveling away from the boundary have a distribution characteristic of the boundary temperature, which differs from the distribution of phonons traveling in the opposite direction more than the difference found deep within the medium. This results in an increased departure from equilibrium locally within the phonon system and an increased gradient in the directionally averaged phonon energy. This is called the temperature slip phenomenon, and is well documented theoretically for gas molecules, photons, and phonons. It occurs within a length scale of the boundary comparable with the mean free path. The magnitude of the temperature slip, specifically the difference between the boundary temperature and the extrapolation of the linear temperature distribution deep within the medium, is approximately the product of the heat flux and the ratio of the mean free path and the bulk thermal conductivity. This argument is based on the Rosseland diffusion approximation.[39] The near-boundary predictions of atomistic simulations should be compared with the solutions to the phonon transport equation in the vicinity of boundaries, or at least to the closed-form expressions for the temperature slip phenomenon.

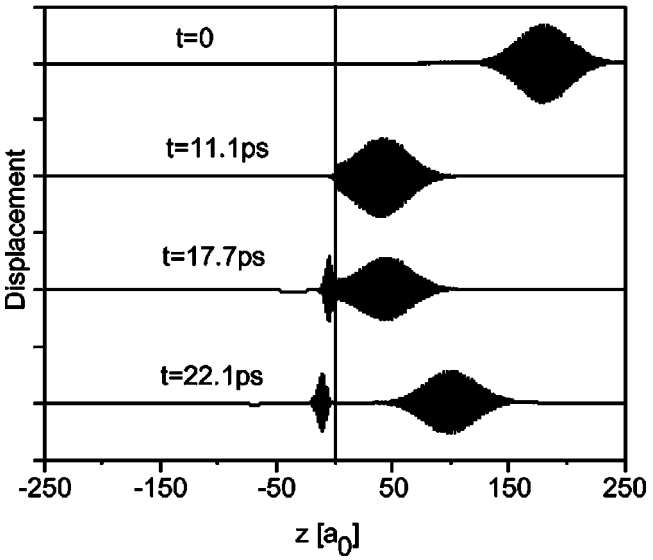

FIG. 4. Interaction of a wavepacket of longitudinal acoustic phonons [$\omega \approx 8.7$ THz, $k_z \approx 0.62(2\pi/a)$] with an (001) epitaxial interface between two diamond-structured lattices differing only in the mass of the atoms (mass $=1$ on the right of the interface, mass$=4$ on the left of the interface); 37% of the energy in the incoming acoustic phonon package is transmitted in the form of a slow-moving optical phonon, while the remaining 63% is reflected with no change in frequency or wavelength (Ref. 42).

Although the value for the thermal conductance of a particular interface in a particular material may be a useful quantity to know, it provides no mechanistic information. The explicit relationship between the temperature-dependent thermal conductance, $G_K(T)$, and the phonon transmission coefficient at an interface has been given by Young and Maris:[40]

$$G_K(T) = \int d\omega C(\omega, T) \langle v_z(\omega) \rangle \langle t(\omega) \rangle \tag{2}$$

where $C(\omega, T)$ is the specific heat, which can be determined from the phonon density of states and the Bose–Einstein distribution function, $v_z(\omega)$ is the component of the phase velocity of the phonon normal to the interface and $t(\omega)$ is the transmission coefficient. The $\langle\ \rangle$ denotes an average over all bands and over all $\mathbf{k}$ vectors (i.e., for both normal and off-axis incidence). While the specific heat and phonon phase velocity can be determined quite easily from the phonon dispersion curves of a perfect crystal, determination of the phonon transmission coefficient requires a detailed analysis of the interface.

Young and Maris[40] determined $\langle t(\omega) \rangle$ for a nearest-neighbor spring model of a fcc lattice with different masses and spring constants on the two sides; this has recently been extended to a disordered interface.[41] In both studies, it was found that $\langle t(\omega) \rangle$ decreases almost uniformly with increas-

ing ω. These results are rather different from a naive implementation of the acoustic mismatch model, which would predict a weak dependence on frequency up to a cutoff frequency determined by the maximum frequency available to the softer material. A simple analytically tractable model that captures the basic features of the frequency dependence in the phonon transmission coefficient would be of great use.

The experiments described in Sec. II B point to the potential capabilities of methods in which phonon packets of well-defined wave vector and polarization are launched towards individual interfaces. Recently, Schelling *et al.*[42] performed atomic-level simulations of phonon–interface interactions. The basic idea is to launch phonon wave packets of well-defined polarization and wave vector towards interfaces and to analyze the transmitted and reflected phonons. For example, Fig. 4 shows four snapshots in the evolution of a longitudinal acoustic phonon as it approaches, interacts with, and then is partially transmitted through and partially reflected by an interface.[42] Analysis of simulations such as this will allow the atomic-level details of phonon–interface interactions to be elucidated.

As discussed above, computational methods based on applications of Fourier's Law and the Boltzmann transport equation are well developed. While MD simulation holds promise of providing detailed atomic and spectral information on heat flow and phonon dynamics, MD will not replace BTE and Fourier's-law approaches to heat transfer problems in complex materials structures and devices. An important challenge is therefore the development of techniques to incorporate the insights of atomic-level approaches into the high-level approaches; success in this can be expected to result in BTE and Fourier's Law approaches of significantly higher fidelity.

D. What is temperature?

In the above discussions of atomic-level simulation we have swept an important conceptual issue under the rug. The usual definition of temperature is related to the average energy of a system of particles. This definition is for a system in equilibrium, and works even for nanoscale systems. However, our interest is in the transport of heat through nanoscale systems. Can temperature, which is an equilibrium concept, still be invoked in a nonequilibrium process such as heat flow? The answer is affirmative for macroscopic systems: they are so large that one can define a local temperature in each region in space. This local temperature will vary from region to region. Then one finds, for example, that the heat current is proportional to $-\nabla T$. The question "*What is Temperature?*" is really a question about the size of the regions over which a local temperature can be defined. In many semiconductor superlattices, the layer thickness is 2–5 nm. Are these regions large enough to define a temperature?

As discussed above, there have been several molecular-dynamics simulations of heat flow through grain boundaries. The most important conceptual problem raised by these simulations is how to define the temperature at different planes in the simulation cell. The simulations calculate the position $\mathbf{R}_i(t_n)$ and velocity $\mathbf{v}_i(t_n)$ of each atom at each time step. It is a relatively simple task to store the velocities, and compute an average kinetic energy over N steps in time

$$\langle \text{K.E.}_i \rangle = \frac{m}{2N}\sum_n^N v^2(t_n) = \left\langle \frac{1}{2} m v_i^2 \right\rangle. \tag{3}$$

It is found that the averaging must be done over very long times to obtain good statistical average kinetic energies.

How is this simple quantity converted to temperature? The numerical simulations show a sharp drop in the average kinetic energy at the grain boundary, as shown in Fig. 3. Here each point corresponds to the average kinetic energy in a slice of a few unit-cell thicknesses. The sharp drop in kinetic energy, at the grain boundary, is consistent with the idea of Kapitza resistance R_K which assumes the heat current through the boundary is proportional to the temperature drop $\dot{Q} = \Delta T / R_K$. In order to find R_K, the kinetic energy must be converted to a temperature scale.

Because the calculations are entirely classical, with the motion of each silicon atom found from Newton's law, the most obvious temperature scale is provided by the classical expression

$$\left\langle \frac{1}{2} m v_i^2 \right\rangle = \frac{3}{2} k_B T_i. \tag{4}$$

The temperature at each atom at site $\mathbf{R}_i$ is given by T_i. This is the procedure adopted in the MD simulations described above.

However, quantum mechanics provides another possible definition. The collective excitations of the atomic motions are phonons. They have a frequency $\omega_\lambda(\mathbf{q})$ which depends upon the wave vector $\mathbf{q}$ and polarization λ of the phonon. The simulations of Fig. 3 were performed on silicon that has six polarizations for each wave vector. In quantum mechanics the average kinetic energy of the phonons is

$$\left\langle \frac{1}{2} m v_i^2 \right\rangle = \frac{1}{4N}\sum_{\lambda,\mathbf{q}} \hbar\omega_\lambda(\mathbf{q}) \xi^{(i)2}(\lambda,\mathbf{q}) \times \left\langle \frac{2}{e^{\hbar\omega_\lambda(\mathbf{q})/k_B T_i} - 1} + 1 \right\rangle, \tag{5}$$

where N is the number of unit cells which is also the number of $\mathbf{q}$ points. The polarization vectors are $\xi^{(i)2}$. They are normalized so that $\Sigma_\lambda \xi^{(i)2} = 3$. In the limit of high temperature, where $k_B T \gg \hbar\omega_\lambda(\mathbf{q})$ the Bose–Einstein occupation factors are approximated as

$$\frac{2}{e^{\hbar\omega_\lambda(\mathbf{q})/k_B T_i} - 1} + 1 \approx 2\frac{k_B T_i}{\hbar\omega_\lambda(\mathbf{q})}. \tag{6}$$

In this high temperature limit, the quantum relation Eq. (5) becomes identical to the classical Eq. (4). The problem with many simulations is that they are not in the high temperature limit. Silicon has optical phonons of very high energy (62 meV$\approx$750 K). For any temperature between 300 and 1000 K, the two definitions of temperature [Eqs. (4) and (5)] gave very different values for T_i.

Another possible definition of temperature is to remove the zero point motion from the quantum definition, since it is

not a classical effect. This option now makes three possible definitions of local temperature. Which is the correct definition?

An important issue is the size of the region over which temperature is defined. The classical definition is entirely local, and one can define a temperature for each atom or plane of atoms. For the quantum definition, the length scale is defined by the mean-free-path $\ell_{\lambda\mathbf{q}}$ of the phonon. If two regions of space have a different temperature, then they have a different distribution of phonons. The phonons can change their distribution by scattering. The most important scattering is the anharmonic process in which one phonon divides into two, or two combine to one. This process occurs on the length scale of the mean free path. A local region with a designated temperature must be larger than the phonon scattering distance. However low frequency phonons have a long $\ell_{\lambda\mathbf{q}}$, and high frequency phonons have a short $\ell_{\lambda\mathbf{q}}$. For the phonons which carry most of the heat, one can plausibly define an average mean-free-path: This $\ell_{\lambda\mathbf{q}}$ is typically larger than the length of the MD simulation cell: this case is called the Casimir[43] limit. One can scale the results to an infinite sized system using the method of Oligschleger and Schön.[44]

This phonon viewpoint of temperature implies that temperature cannot be defined for a particular atom, or a plane of atoms. In particular, there should not be an abrupt variation in temperature between a plane of atoms. Although this definition seems quite reasonable, it makes the numerical results shown in Fig. 3 quite puzzling. The MD simulations by different groups do show an abrupt change in the kinetic energy of a plane of atoms at the twin boundary. Regardless of which temperature scale is adopted [Eqs. (4) or (5)], a graph of temperature versus distance will show an abrupt change. A possible resolution for this puzzle is that a grain or twin boundary may form a natural boundary for a region of temperature. The statement that temperature cannot be defined within a scale of distance given by $\ell_{\lambda\mathbf{q}}$ may not apply across grain boundaries. The boundaries may provide natural limits to the regions of temperature. Even if one adopts this hypothesis, it still means that temperature cannot vary within a grain, or within a superlattice layer, on a scale smaller than $\ell_{\lambda\mathbf{q}}$. If the layer thickness of the superlattice is less than $\ell_{\lambda\mathbf{q}}$, then one cannot define $T(z)$ within this layer. The whole layer is probably at the same temperature. This point is emphasized, since all theories of heat transport in superlattices have assumed that one could define a local temperature $T(z)$ within each layer.

The results in Fig. 3 may be measurable. X-ray scattering at synchrotron sources can measure the lattice constant of atoms in each atomic layer.[45] The lattice constant can be converted to a local temperature scale for that plane. They should be able to determine whether this quantity has an abrupt change at an interface while heat is flowing. Although this discussion of "*What is Temperature?*" has been cast in the framework of MD simulations, the issues are more general. One of the major issues of thermal transport in nanoscale systems is whether temperature can be defined locally. If it cannot, then how is transport calculated?

Another approach is to adopt a Landauer formalism, and assume there are two thermal reservoirs at known temperatures, and consider the ballistic flow of heat between them. This does not work for most nanoscale devices since the values of $\ell_{\lambda\mathbf{q}}$ are much smaller than the distance between the reservoirs. So heat flow is diffusive rather than ballistic. How do you calculate diffusive heat flow without a local temperature?

As an example of the importance of temperature, we will comment on two related theoretical calculations. Stoner and Maris[10] measured the Kapitza resistance between diamond and other crystals. Between diamond and Pb the heat flow was much higher than could be explained by a purely phonon conduction. Huberman and Overhauser[46] suggested that the conduction electrons in Pb were playing an essential role in the boundary resistance. Phonons from diamond carry heat to the interface, and electrons in Pb carry it away. There have been two different calculations of this process, one by Huberman and Overhauser,[46] and one by Sergeev.[47] The two theories are very different since the two groups made different assumptions regarding temperature. Sergeev assumed that there was an abrupt change in temperature at the boundary between diamond and Pb. His assumption agrees with the conventional view of Kapitza resistance which assumes a temperature step. Huberman and Overhauser assumed temperature could not be defined locally, and there was no step in temperature. The interface region was at one temperature. They used a Landauer formalism to compute the energy exchange between electrons and phonons. Which of these two different theories is better depends on whether a grain boundary can support an abrupt change in temperature.

E. Transport theory

Most theories of transport in solids employ the Boltzmann transport equation (BTE). For both electron and phonon transport, the form of the equation, and the form of the various scattering mechanisms, are very well known. This theory can explain, in bulk homogeneous materials, the dependence of the electrical conductivity, the thermal conductivity, and the Seebeck coefficient, on temperature, impurity content, isotope scattering, and quantum confinement.

However, the Boltzmann equation treats the electrons and phonons as classical particles. One is solving, say for phonons, for the density $f[\mathbf{r},\omega_\lambda(\mathbf{q}),t]$ of excitations with polarization λ, wave vector $\mathbf{q}$, frequency $\omega_\lambda(\mathbf{q})$ at point $\mathbf{r}$ at time t. The wave nature of the excitation is neglected, as is any interference phenomena caused by the wave nature of the phonons. Furthermore, the scattering rates in the BTE are calculated assuming the system is only slightly perturbed from equilibrium. The solutions to the BTE assume the existence of a local temperature. Neither of these two assumptions may be valid in nanoscale devices.

Wave interference becomes important in nanoscale devices. The wavelengths of the phonons are similar to the length scale of the microstructure. At room temperature, in most solids, all of the phonons states in the Brillouin zone are involved in the transport. Their wavelengths span the range from atomic dimensions to the size of the sample. Most of the actual heat is carried by the phonons with wave lengths of a few nanometers. On this scale wave interference

becomes important in transport. Similar considerations apply to electron transport in nanoscale devices. Since the traditional Boltzmann equation cannot deal with these phenomena, other theoretical approaches are required.

One method is to calculate the phonon states for the actual microstructure, and use those states in the BTE. For transport in a superlattice, the frequencies $\omega_\lambda(\mathbf{q})$ are those of the phonons in the superlattice. This approach inserts in some of the wave phonmena. The phonon states depend significantly on the interference due to scattering from the multiple layer boundaries of the superlattice. One problem with this approach is that it ignores an important phenomenon. Most scattering effects contribute to a finite mean-free-path which has a major effect on the phonon frequencies in the superlattice. Solving this problem using the BTE is also complicated by phonon band folding. There are many superlattice bands, phonons scatter between them, and the BTE becomes a matrix equation of large dimension. This calculation is quite ambitious and has never been done. This does not include all wave interference phenomena.

Another possibility is to use the quantum Boltzmann equation[48] to solve for the distribution $f(\mathbf{R},t:\omega,\mathbf{q})$. Compared to the BTE, there is one more vector variable in the argument that makes the solutions more complex. This more fundamental equation does include wave information. However, it is difficult to solve and is seldom used. One problem is the choice of boundary conditions to apply on the surface of the system in order to connect it to a heat reservoir. This issue has been much discussed in the literature on electron flow in nanoscale devices.[49,50]

If one throws out the concept of a local temperature, so that the BTE cannot be used, then there is no known way to solve this important problem. Many semiconductor devices are dependent upon the electrical currents provided by the electrons. The heat currents have components from both electrons and phonons. Presently there is no accurate way to model the heat flows in these nanoscale systems while including the exchange of heat between electrons and phonons. A major theoretical challenge is to invent a new method of solving this and related transport problems.

III. PHONONS AND THERMAL TRANSPORT IN NANOSCALE STRUCTURES AND DEVICES

A. Silicon films and devices

1. Conduction along semiconducting monolayers

Phonon conduction along single- and polycrystalline monolayers is important for silicon-on-insulator (SOI) circuits,[51] novel 3D multilayer electronics,[52] and MEMS with semiconducting or dielectric membranes.[53] Silicon monolayers have received the most attention, either as suspended membrane (a geometry relevant for many thermal microsensors) or embedded between amorphous silicon dioxide films (as in SOI transistors). In the second geometry, the surrounding silicon dioxide films act as diffuse phonon emitter absorbers and provide a boundary condition that resembles phonon scattering on the boundaries of a membrane with roughness above a few angstroms. This situation differs from that in superlattices with comparable phonon mean free path on both sides of each interface, for which conduction is influenced by the coupled ballistic phonon transport in adjacent layers, see Sec. IV. (A macroscopic version of this geometry has been used by Pohl and co-workers[54] to study phonon scattering in thin films at $T<1$ K.)

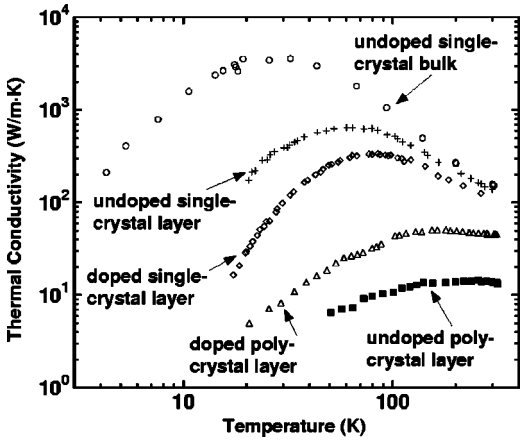

FIG. 5. Overview of thermal conductivity data for silicon films with varying microstructural quality and impurity concentrations after Ref. 58. The data illustrate the relative importance of phonon scattering on film and grain boundaries and impurities. The data for undoped single-crystal bulk samples are taken from Ref. 59. Both single crystal films have thickness of 3 μm, and for the doped film, a boron concentration of 10^{19} cm^{-3}. (Ref. 55). The undoped and doped (1.6×10^{19} cm^{-3} boron) polycrystalline films have grain sizes of 200 and 350 nm, respectively (Refs. 57 and 58).

Figure 5 shows that for single-crystal silicon films, phonon-interface scattering strongly reduces the effective thermal conductivity at low temperatures. For single-crystal silicon layers doped at concentrations higher than 10^{17} cm^{-3} the conductivity is reduced by scattering on impurities and free electrons.[55] Figure 5 shows that this is particularly important at low temperatures. Measurements at 20 K on layers of thickness 3 μm with phosphorus and boron concentrations of 1.0×10^{18} cm^{-3} yielded reductions by approximately two and four, respectively, with the difference resulting from the disparity in mass of the two impurity types. At room temperature, measurements along silicon films of thickness down to 74 nm showed a reduction of the conductivity by a factor of two compared to bulk data.

In polycrystalline silicon films, phonon scattering on grain boundaries and related defects dominates over scattering from the surface or the film/substrate interface. Polysilicon conductivities are reduced compared to those of pure crystalline films,[56] but the roles of impurities and grains are difficult to separate. Recent work studied films with grain sizes between 300 and 500 nm, extracted using transmission electron microscopy, and boron or phosphorus concentrations up to 4.1×10^{19} cm^{-3}, measured using secondary ion mass spectroscopy (SIMS).[57,58] Figure 5 shows that polysilicon conductivities are reduced strongly at all temperatures compared to similarly doped single-crystal silicon layers, which illustrates the importance of grain boundary scattering. The grain structure and spatial impurity distribution depend strongly on the temperature and duration of annealing. Annealing of the doped polysilicon film and the resulting

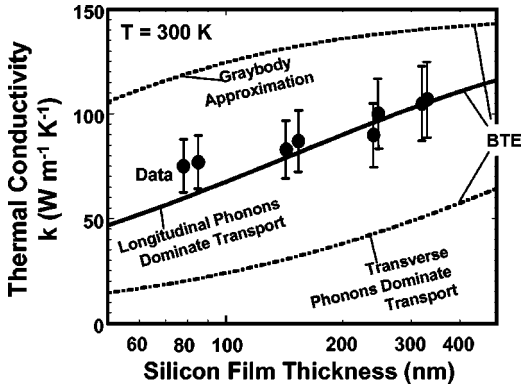

FIG. 6. Experimental data for the effective room-temperature thermal conductivity along silicon films of thickness near 100 nm (Ref. 64). The data are compared with predictions based on the Boltzmann transport equation engaging different assumptions about the frequency dependence of phonon relaxation times and the relative contributions of the phonon branches to conduction.

increase in grain size yields a higher thermal conductivity than that of the undoped film.

The conduction size effect along crystalline and polycrystalline monolayers at low temperatures can be effectively predicted using a semiclassical approach, based on solutions to the Boltzmann transport equation for conduction along films[60] and based on a spectrally-resolved form of the expression $\kappa = Cv\ell/3$.[61] In this expression, C is the heat capacity per unit volume and v and ℓ are the phonon velocity and mean free path, respectively. Polysilicon data are effectively predicted below about 10 K by reducing the mean free path using Matthiessen's rule[62] and a grain-boundary free path given by d_G/B, where d_G is the grain size and B is a dimensionless constant governed by the grain shape and grain boundary reflection coefficient. Polycrystalline diamond films are worthy of brief discussion here because they illustrate another way in which grain boundaries can reduce phonon conduction. The free path d_G/B is overly simplistic for diamond film data owing to the large concentration of other imperfections. Because imperfections populate primarily at grain boundaries, the phonon scattering rate can still be coupled to the grain size d_G using a semiclassical approach.[63]

The anisotropy and nonlinearity of phonon dispersion relationships complicate predictions above 100 K for GaAs, Ge, and AlAs films, and above 150 K for silicon films owing to its higher Debye temperature. The predictions become more challenging because phonon dispersion induces differences in transport among the various phonon modes and directions. Figure 6 illustrates this issue for transport along silicon films of thickness near and below 100 nm. Predictions are performed under a greybody assumption, which overestimates the fraction of phonons contributing to heat transfer and therefore underestimates the phonon mean free path and the thermal conductivity size effect for a film of given thickness. Predictions are also provided with spectrally varying mean free paths under the competing assumptions about which phonon modes are dominating conduction in the material.

2. Monte Carlo solutions of the Boltzmann transport equation

The problem of phonon transport considering dispersion effects has been addressed using Monte Carlo simulations, which are essentially an alternative approach to solving the Boltzmann transport equation. The Boltzmann transport equation (BTE) describes heat flow by phonons in nonmetallic solids, when wave effects are negligible. The BTE, in its most general form, is difficult to solve analytically for realistic phonon dispersion and density of states as well as for transitions between phonon polarizations and for irregular geometries.[65] Recent work-by Majumdar,[26] Chen and Tien,[66] Goodson,[63] and Chen[67] have used analogies from radiative heat transfer and presented solution strategies for both the diffusion and the ballistic limit. In such calculations, however, phonon dispersion was neglected, and a single ''average'' polarization branch was considered. Furthermore, such calculation strategies can only be adopted for considerably simplified geometries. If all these assumptions are removed, it is extremely difficult to solve the BTE for phonons by a deterministic approach in an arbitrary geometry. This is because the number of independent variables is too large, and would render any kind of discretization scheme too complex to be practical. Furthermore, the phonon–phonon scattering events are difficult to incorporate without a simplifying relaxation time approximation.

One approach to capture the complexity of phonon transport in the particle regime is to use Monte Carlo or stochastic simulations to solve the BTE. Over the last decade there has been tremendous advancement in the development of Monte Carlo solution techniques for the BTE for electrons and holes in semiconductors.[68–72] However, there have been very few reports of using Monte Carlo simulations for phonon transport.[73,74] These studies have either assumed the Debye approximation for density of states or did not consider phonon–phonon interactions. More recently, Mazumder and Majumdar[75] considered phonon dispersion as well as various phonon scattering mechanisms to study heat transport in complex geometries and to predict the thermal conductivities. The result showed that by fitting one parameter using experimental data of thermal conductivity at one temperature, predictions of the thermal conductivity of silicon agreed well with experimental data over a wide temperature range. In addition, it was able to capture phonon transport in both the ballistic and diffusive limits. Despite the success of this approach, one must be aware of the challenges in applying this approach more generally to problems in nanoscale thermal transport.

First, it must be recognized that it is difficult to capture all the selection rules for transitions between polarizations during phonon–phonon interactions. For example, the transitions between longitudinal and transverse acoustic phonons as well as those between acoustic and optical phonons are very important in energy dissipation and thermal transport. Mazumder and Majumdar[75] ignored the selection rules and obtained local phonon distributions in different polarizations based on a quasiequilibrium condition. For highly nonequilibrium cases, this approach cannot be applied. Hence, it is extremely important to develop schemes for capturing tran-

sitions between polarizations during phonon–phonon interactions. Second, the relaxation times for phonon–phonon interactions have, in the past, been used only for bulk solids and only for the most common materials. These were obtained from approximate analytical solutions that require fitting parameters. For example, the phonon scattering relaxation times for silicon are generally obtained from Holland.[61,76] These cannot be used when silicon is nanostructured which can modify the phonon dispersion relation. For many other materials, relaxation times are not available even for bulk solids. Hence, there is a need to develop approaches of predicting the relaxation times for arbitrary phonon dispersion relations. This would allow one to study energy dissipation and thermal transport in nanostructured solids such as quantum dots, nanowires, films, and superlattices, where the phonon dispersion relations are modified due to confinement or wave interference. If both these challenges are overcome, Monte Carlo simulations of phonon transitions and transport can be an extremely effective tool to study nanoscale energy dissipation and thermal transport.

3. Nanoscale hotspots in devices

The phonon-boundary scattering discussed above for silicon monolayers is only the first among three nanoscale effects which complicate heat conduction from metal-oxide-semiconductor (MOS) transistors. Two additional nanoscale effects result from the small size of the region of electron energy transfer to the lattice. Before describing these effects, it is important to note that all three are augmenting the departure from equilibrium of the phonon distribution functions, rendering the usefulness of a phonon ''temperature'' more questionable. Theoretical treatments of these effects use temperatures either for the phonon system as a whole or for fractions of the phonons sharing comparable group velocities; this approach can at best be viewed as a shorthand placeholder for energy density. This situation may eventually be remedied through detailed phonon transport analysis or molecular dynamics, although the computational demands will be excessive owing to the three-dimensional nature of the problem.

Electrons traveling between the source and drain are accelerated by the electric fields and generate primarily optical phonons. Simulations of electron transport using drift diffusion and the more rigorous Monte Carlo or hydrodynamic approaches[77,78] illustrate that rates of phonon generation are sharply peaked on the drain side. The region with strong lattice heat generation has dimensions near tens of nanometers and is much smaller than the channel length (50–150 nm depending on the technology generation of interest) and the phonon mean free path, $\ell \approx 250$ nm according to Ref. 64. This second nanoscale effect, which we will call hotspot ballistic emission effect, causes the temperature of the phonon ''hotspot'' to be larger than that predicted using diffusion theory, by a factor comparable with ℓ/r where r is the hotspot dimension.[79] While the precise distribution of the generated phonons between the optical and acoustic modes depends strongly on the energies of scattering electrons, it is clear that the generated phonons have group velocities far below the velocity characteristic of heat conduction by the lattice. The generation of high concentrations of optical phonons within a region with dimensions small compared to the mean free path causes a third nanoscale effect, which in the present manuscript we will call the hotspot far-from-equilibrium effect.

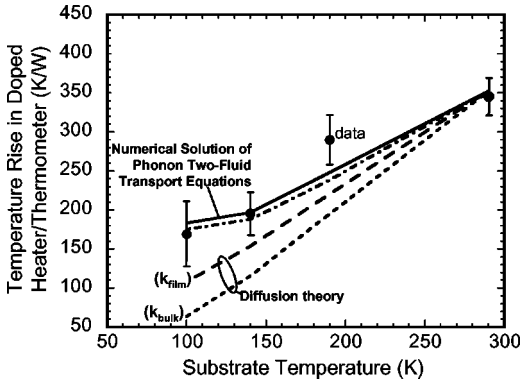

FIG. 7. Experimental data for the phonon temperature rise within a resistive heater in silicon with dimensions (at low temperatures) smaller than the phonon mean free path. The data are compared with predictions based on diffusion theory, the two-fluid phonon Boltzmann transport equation, and a simple resistance model based on the ratio of the square of the mean free path and the effective cross-sectional area of the heat source (Ref. 81).

Sverdrup[80,81] examined this third nanoscale effect experimentally using a dedicated microstructure and theoretically by breaking the phonons into two propagating and stationary groups. The theoretical treatment solved the Boltzmann transport equation for the propagating phonons together with a reservoir energy-storage equation for the stationary phonons. Stationary phonons were generated by electron scattering, with a spatial distribution taken from an independent analysis of the electron and hole transport problem in the transistor. Simulations of a SOI transistor with channel length 150 nm concluded that the peak lattice temperature (a weighted average of the temperatures of the stationary and propagating phonons) was elevated by more than a factor of two compared to predictions based only on the heat diffusion equation. This difference resulted in part from the localized transfer of energy from phonons with relatively small group velocities to those at lower energies, which dominate heat conduction.

This third nanoscale effect was examined experimentally using localized heating by a doped silicon bridge within a suspended silicon membrane. Experimental data and predictions for the temperature of the bridge are provided in Fig. 7. The cross-sectional dimensions of the doped heater were $\approx 1\ \mu$m and much larger than the phonon mean free path at room temperature, such that all of the predictions and the data are consistent with simple diffusion theory. At lower temperatures, where the phonon mean free path is longer, the dramatic departure from equilibrium induced by optical phonon generation within the hotspot (far-from-equilibrium effect) becomes important. Predictions at low temperatures using the Boltzmann equation with the stationary and propagating phonon groups agree reasonably well with the data, and are consistent with a simple closed-form expression in which the excess temperature rise scales with $(\ell/r)^2$.

The hotspot effect, discussed above for silicon, could very well be much larger in optoelectronic devices because of the phonon band structure in the associated semiconducting materials. In polar semiconductors, such as GaAs, the carriers interact predominantly with LO phonons of wave vector $q \approx 0$.[82] Thus, carrier cooling leads to the generation of nonequilibrium modes for which the group velocity is exceedingly small, i.e., to a nanoscale hot spot. This so-called hot-phonon effect is believed to be responsible for the reduction of the cooling rate of electrons at densities higher than 10^{17} cm^{-3}.[83] It is well known that the presence of interfaces changes the character of the optical phonons in that they are no longer purely LO or transverse-optical (TO) but a mixture involving LO, TO, and interface modes.[84] Since mixing results in larger dispersion, this suggests that structure engineering can be applied to attain large group velocities to facilitate the removal of LO heat from the device active region. In the bulk, heat diffusion relies on the spontaneous decay of the optical phonons into the more movable acoustic phonons.[85] Recent progress in the generation of coherent high-frequency acoustic modes,[86] which can be used to stimulate LO decay, hold promise for applications in nanoscale heat removal.

B. Nanostructures with tailored phonon transport properties

Unlike bulk materials, the phonon properties of semiconductor nanostructures and, in particular, the phonon frequency, group velocity, spectral density as well as the strength of the interaction with carriers, can be widely modified to improve the performance of optoelectronic and other devices. In some cases, it is desirable to increase the electron–phonon interaction; an example is the interband semiconductor laser, where fast relaxation rates reduce hot electron effects.[87] On the opposite side, we have devices such as mid-infrared emitters and detectors based on intersubband transitions, for which a reduction of the electron-phonon coupling constant is advantageous because it leads to larger lifetimes of the relevant excited states.[87] An important example of the effect of quantum confinement on scattering rates is that of the phonon bottleneck in quantum dots. This refers to the strong suppression of the electron relaxation rate which arises when the energy spacing of the confined carriers exceeds the energy of the longitudinal optical (LO) phonon.[88]

C. Phonon transport in 1D nanostructures

One-dimensional (1D) nanostructures such as carbon nanotubes and semiconductor nanowires have recently received a lot of attention. While most of the current research is being focused on electronic and optical properties, thermal transport is also of interest for basic science as well as for technological applications. For example, Schwab *et al.*[89] demonstrated quantum thermal conductance in nanofabricated 1D nanostructures, where the quantum of phonon conductance, G_{ph}, is given

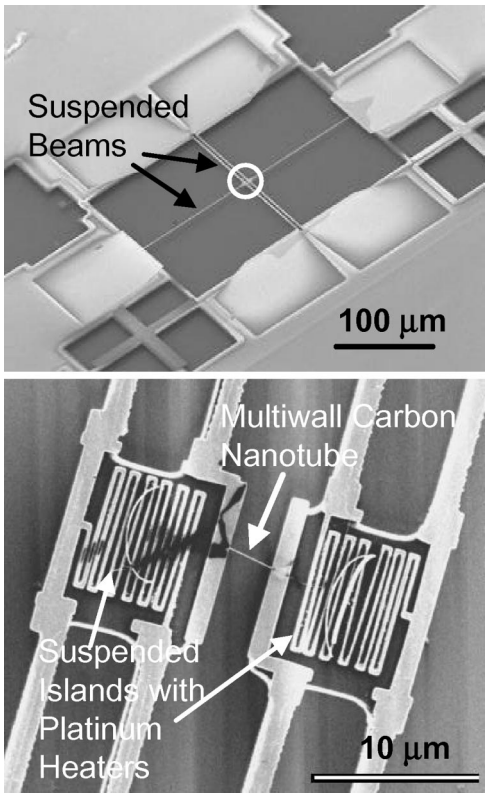

FIG. 8. A large scale scanning electron microscopy image of a microfabricated device (left). Two independent islands are suspended by three sets of 250 μm long silicon nitride legs with Pt lines that connect the microthermometer on the islands to the bonding pads, (right) Enlarged image of another design of suspended islands with the Pt thermometer and heater fabricated by electron beam lithography. Also shown is an individual multiwall carbon nanotube, 14 nm in diameter, bridging the two islands (Ref. 94).

$$G_{ph} = \frac{\pi^2 k_B^2 T}{3h}, \tag{7}$$

where k_B is the Boltzmann constant, T is the absolute temperature, and h is the Planck constant.

In this regime, a 1D nanostructure behaves essentially like a phonon waveguide similar to optical ones for light. Berber[90] and Osman and Srivastava[91] have theoretically predicted very high thermal conductivity for carbon nanotubes. In addition, Hicks and Dresselhaus[92] have suggested that quantum confinement of electrons in nanowires could be used to manipulate thermoelectric properties, which could be useful for solid-state energy conversion devices. Hence, it is important to study thermal transport and energy conversion in 1D nanostructures.

On the experimental side, there have been some recent attempts[93] to measure the thermal conductivity of a collection or a mat of carbon nanotubes. However, due to weak coupling between carbon nanotubes, the measured thermal conductivity was found to be much lower than that predicted.[90] Kim[94] developed a microdevice (see Fig. 8) containing two adjacent silicon nitride (SiN_x) membranes or islands suspended with long thermal isolation legs. Each island contains a Pt resistor which can be used as both a heater and a thermometer. A nanowire can be placed in between and

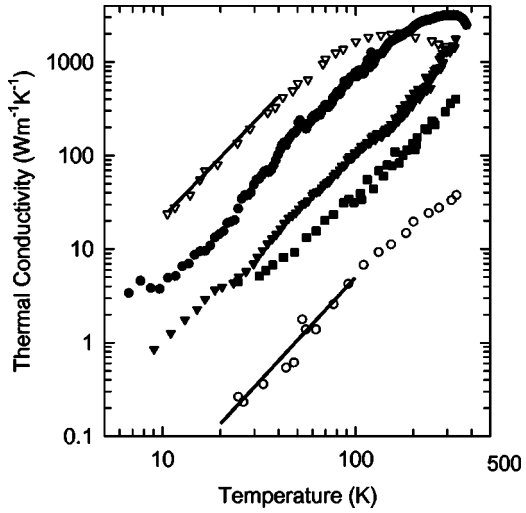

FIG. 9. Measured thermal conductivity of a 14 nm diameter multiwall carbon nanotube (MWCN) (solid circle), an 80 nm diameter MWCN bundle (solid triangle), and a 200 nm diameter MWCN bundle (solid square) (Ref. 94). Data for two vapor-grown graphite fibers (Ref. 95), one heat treated to 3000 °C (open triangle) and one without heat treatment (open circle) are included for comparison. The lines represent the calculated (Ref. 95) basal-plane thermal conductivity of graphite, assuming temperature-independent low-temperature phonon mean free path $\ell = 2.9\ \mu$m (upper line) and $\ell = 3.9$ nm (lower line).

bridge the two suspended islands. One of the islands is heated to a temperature T_h, which is determined by measuring the resistance of the Pt wire on the island. Conduction through the nanowire heats the sensing island to a temperature T_s, which is also measured by resistance thermometry. By noting the power dissipated by the heater, Q_h, and estimating the thermal conductance of the suspended legs connected the islands in the absence of a nanowire, the conductance of the nanowire G_n can be calculated.

Figure 9 shows the plot of thermal conductivity of a multiwall carbon nanotube (MWCN) as a function of temperature measured by this technique. The T^2 temperature dependence suggests that MWCN behaves thermally as a 2D solid; the MWCN has a thermal conductivity of about $3000\ \mathrm{W\,m^{-1}\,K^{-1}}$ at room temperature, which is in close agreement with the predictions of Osman and Srivastava.[91] Note that the measured value includes the contact resistance between the nanotube and the two islands, although it is predicted to be lower than the resistance of the tube itself. Estimation of the contact resistance has remained a challenge. Nevertheless, it is envisioned that this technique can be used to measure thermal conductivities of a variety of semiconducting or metallic nanowires that are technologically important.

Phonon transport in 1D nanostructures offers the opportunity to understand the basic science of phonon dynamics and transport, while allowing the ability to manipulate thermal properties. Phonons in nanowires can be different from those in bulk semiconductors mainly because the dispersion relation could be significantly modified due to confinement in two directions. In addition, the presence of a surface can introduce surface phonon modes. These result in many different phonon polarizations other than the two transverse and one longitudinal acoustic branches found in bulk semiconductors. Such changes in the dispersion relation can modify the group velocity and the density of states of each branch. The phonon lifetime also changes and this arises from two sources. First, the phonon–phonon interactions can change because selection rules based on energy conservation and wave-vector relations depend on the dispersion relation. Second, boundary scattering can be much stronger in nanowires (5–50 nm diameter) than in bulk semiconductors. While there have been some theoretical studies on phonon conduction in nanowires,[96,97] there are still several open questions regarding phonon transport in 1D nanostructures: What are the phonon–phonon relaxation times and the selection rules? How does the phonon gas couple to the electronic one? What is the role of individual defects in a nanowire on phonon transport and does the presence or absence of single defects alter overall thermal transport? How can nanowires be designed for very high or low thermal conductivities? It is envisioned that these questions can only be answered by a combination of experimental studies of single nanowires and theoretical and computational (molecular dynamics and Monte Carlo simulation) studies of phonon transport in 1D nanostructures.

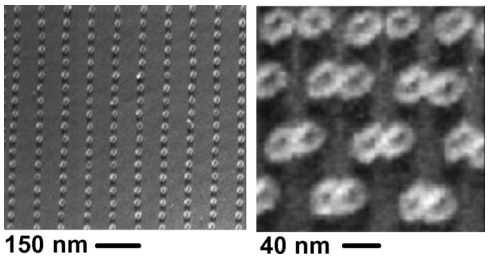

FIG. 10. Images of divots written in a polymer film using heat and force applied by a silicon atomic-force-microscope (AFM) cantilever. The images are recorded using the same cantilever used during the writing process and a thermal reading technique involving heat conduction from the cantilever into the substrate (Ref. 53).

D. Nanoscale 3D conduction and mass transport in polymers

Section III focused on heat transport in crystalline or nearly crystalline materials. Recent developments in data storage technology highlight important shortfalls in our understanding of nanoscale heat and mass transport in disordered materials such as polymers. In thermomechanical data storage, a heated AFM cantilever forms a divot with radius of curvature below 20 nm in a polymer film of thickness near 30 nm on a silicon substrate.[53] Figure 10 illustrates divots written in a polymer film, as observed using an AFM-based thermal readback mechanism. The transport of heat and mass in the vicinity of the cantilever tip governs the bit writing rate and bit size; therefore, nanoscale transport properties are the critical figures of merit. Fundamental study is motivated by the fact that the thickness of the polymer film and the radius of curvature of the divot are more than an order of magnitude smaller than the radius of gyration of the polymer in bulk form. Therefore, heat flow and deformation within

the polymer will be strongly influenced by the partial orientation of molecular strands in the plane of the film.

While the theory of polymer motion has evolved much in the past two decades,[98,99] there is little theory and data of direct relevance to the three-dimensional motion observed during bit formation. The three-dimensional, multiscale (10–100 nm) nature of the conduction problem within the cantilever and into the polymer film may well render it beyond the reach of atomistic simulations for a number of years. Furthermore, semiclassical phonon simulations such as the Boltzmann equation and Monte Carlo techniques, while appropriate in the silicon cantilever tip, are of little use in the disordered polymer. Modifications of continuum theory to account for anisotropy and partial orientation of molecular strands provide some help with the heat transport problem,[100] and may become more accurate when coupled with atomistic simulations of individual molecules.

IV. THERMAL TRANSPORT IN NANOSTRUCTURED MATERIALS

In this section we consider bulk or thin film materials that contain a collection of nanostructured units. This includes amorphous or glassy materials, materials with nanoscale grains, as well as nanoporous materials that contain voids on the order of a few nanometers. Also included in this category are multilayer films as well as epitaxial superlattices, which include a collection of nanometer-scale films stacked on each other. The common feature in these materials is that one can identify a nanostructured unit as the building block. For example, in amorphous materials the local ordering is on the scale of lattice constants while for epitaxial superlattices the unit is a superlattice period.

While phonon dynamics and transport in a single unit is important and must be studied, the collective behavior of a large number of units can add to more complexity, i.e., there may be some collective modes which are not found when considering only single units. For example, when the phonon coherence length scales are larger than the size of the unit, phonon interference effects lead to modified dispersion relations. Hence, the appearance of both wave effects at nanoscales and diffusive heat flow at bulk scales poses challenges in predicting thermal transport in these materials.

Such predictions are important because nanostructured materials find many applications. For example, with the size of electronic devices shrinking it is necessary to use materials with low dielectric constants. Amorphous or nanoporous materials are generally chosen for this purpose, although their thermal conductivities are very low which results in poor thermal management. Can materials with low dielectric constants and high thermal conductivity be designed? This can be answered if we have a fundamental understanding of phonon dynamics and transport in such materials. Refractory ceramic films are also used in thermal barrier coatings in gas turbine engines. The performance of such engines can be significantly improved if the thermal conductivity of these films can be reduced, thus allowing operation at higher temperatures. Finally, epitaxial superlattices of semiconductor films are under intense investigation for thermoelectric energy conversion devices because they offer the ability to the control both electronic band structure and phonon transport.

A. Amorphous and nanoporous materials

Heat transport is an important problem to the semiconductor industry, which is manifested in at least two key areas: advanced packaging and device reliability. In the former case, the challenge is how to maintain acceptable operating temperatures with an increasingly dense circuit layout operating at increasingly higher frequencies. In short, the package cooling requirement for silicon logic devices is projected to be greater than 175 W after 2010.[101] The package thermal problem is amplified when one considers that the increasingly widespread proliferation of logic chips requires flexible package platforms for applications ranging from appliances and personal digital assistants at one extreme to the high compute node density required in modern server farms. Hybrid, chip-on-chip, and three dimensional chip construction adds to the package complexity that must be addressed. Furthermore, as performance requirements increase, as the number of I/O's multiplies, and as the clock frequencies move above 10 GHz, a shift toward optical interconnects probably becomes inevitable. If so, an additional thermal problem will be realized because optical transmitters will need to be integrated into the package or perhaps on-chip. Research into new ways to improve the package thermal performance is ongoing, much of which relies on novel opportunities offered by nanostructured materials. Examples range from high thermal conductivity package fill or epoxy using nanotube composites to chip-scale integrated thermoelectric refrigerators.

The device reliability thermal problem refers most importantly to the reduction in electromigration lifetime for metallic interconnect systems, in which metal mass flow occurs in response to electrical current carried in the interconnects until the metal line fails with a high resistance condition. CMOS technology at dimensional scales below 0.25 μm has significant performance limitations due to RC delays in the interconnect network, so much so that the traditional Al based metallization has been discarded in favor of Cu and Cu alloys and the silicon dioxide interlayer dielectric materials are being replaced by more exotic materials with lower dielectric permittivity. In the latter case, SiO_2 thin films with a relative permittivity $\epsilon_r \approx 4$ is forecast to be replaced in a stepwise fashion by materials with $\epsilon_r \approx 3$ and soon after that by materials with $\epsilon_r \approx 2$. This transition is being made at a rate limited by our understanding and control of the microscopic and processing properties of the films.

The advantage offered by these new insulator materials has a concomitant set of problems, not the least of which is an amplification of the self-heating problem. Low permittivity materials generally have low thermal conductivity, the consequence of which is an increase in the operating temperature of the metallic traces, leading to reduced electromigration resistance and premature circuit failure. Shen[102] published a straightforward calculation that clearly demonstrates this self-heating issue. Examining a multilevel metallization idealization employing Cu and polyimide, as a prototypical low permittivity material, the temperature increase in interconnect system was calculated as a function of the number of

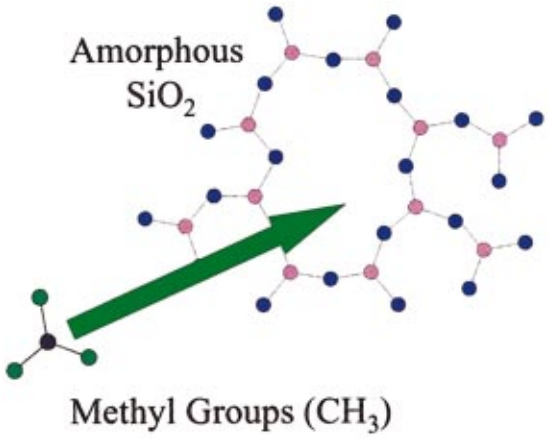

FIG. 11. (Color) Schematic representation of methyl doping of an amorphous SiO_2 network.

metal layers in the design. For only a six layer system, typical of today's logic designs, the increase of temperature easily exceeded self-heat temperature limits currently in use. Future designs will include more metal layers. Furthermore, given that logic circuit design employs a wide range of local metal densities, it is likely that Shen's model underestimates the reliability jeopardy.

Given the above considerations, understanding the thermal conductivity of thin ($\sim<500$ nm) interlayer dielectrics is of considerable interest. Using an example, consider the properties of carbon doped silicon dioxide (CDO).[103] A schematic representation of these materials is presented in Fig. 11, in which the sp^3 network of the amorphous oxide is opened up by the introduction of chemical moieties, such as the methyl group suggested in the figure. The thermal conductivity of a set of these materials has been measured using the time domain thermoreflectance (TDTR) method,[104] and the results in two cases independently validated using an electrical resistance measurement and full scale finite element thermal modeling method.[105] The results are summarized in Fig. 12, in which the measured thermal conductivities of thermally grown oxide, plasma enhanced TEOS oxide, fluorine doped SiO_2, a-SiC, and various forms of CDO are compared to the measured oxide mass densities, determined using x-ray reflectometry. (The a-SiC samples are actually a carbon rich CDO material.) The variability of this measurement is estimated to be $\sim 5\%$ determined by testing multiple samples and over a period of ≈ 1 year. For this family of materials the introduction of carbon is the most important factor correlated to the drop in thermal conductivity. The preparation method and the chemical precursor produce smaller changes in thermal conductivity. Carbon doping, in turn, reduces the resultant mass density of the film, an effect which is amplified by the inclusion of $(CH)_x$ moieties for $x=1$, 2, and 3 in the amorphous network.[106,107] Note also that F doping has the same density reducing effect, albeit smaller in magnitude.

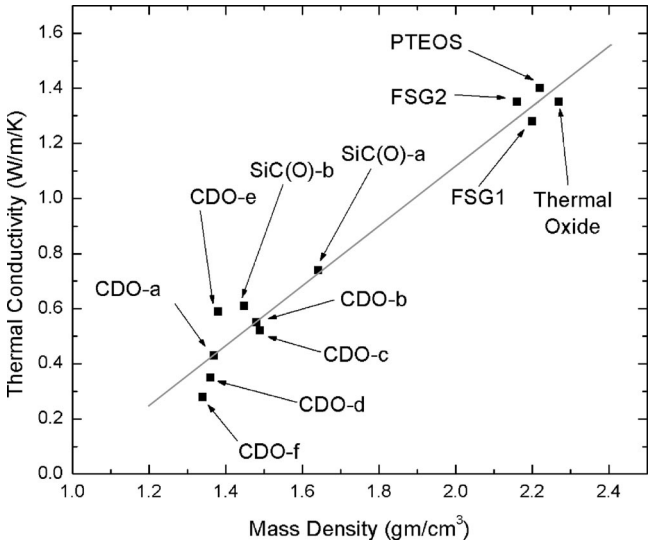

FIG. 12. Room temperature thermal conductivities of carbon-doped silicon dioxide (CDO) films measured using time domain thermal reflectance TDTR. (The linear fit is merely a guide for the eye.)

The minimum thermal conductivity theory of Cahill and Pohl[108] has been applied to these results to derive thermal conductivities. This model is an attractive option because it depends only on the atomic number density and sound velocity of the films. However, using the sound velocity derived from the elastic modulus measured separately using nanoindentation for each film, the results obtained show only a qualitative agreement with experiment, with errors of $\pm 30\%$. A more successful approach would not only close the gap between model and experiment but, for technological relevance, also include the effects of local chemical bonding and deposition process methodology.

The CDO materials described above are interesting in that the network is generally an sp^3 bonded one, in which the material density is reduced by configurational rearrangement to accommodate the dopant materials. The resultant molecular cage-like pores are on the atomic scale and probably do not require explicit consideration in an elementary theoretical description. However, more aggressive materials, those providing a dielectric permittivity near 2, can be prepared using the explicit introduction of nanoscale porosity and alternative local chemistry. The manner in which one includes nanoscale pores into a theoretical approach for thermal transport is not yet precise. For example, the description of the transition from ''cage-like'' to nanoporosity needs to be clarified. Perhaps more importantly, the pore sizes of interest, which are a few nanometers so as not to limit the mechanical strength of the films, are comparable to the relevant thermal phonon wavelengths, which renders continuum approximations suspect. The effect of porosity on the room temperature thermal conductivity of xerogel, a nanoporous form of a-SiO_2, was recently studied by Hu and co-workers;[109] they proposed phenomenological two-phase mixture models that usefully describe the dependence of the conductivity on porosity.

To explore the effect of porosity on the thermal transport in lower permittivity amorphous materials, Costescu *et al.*[110] have investigated the thermal conductivity of hydrogen–silsesquioxane (HSQ) films in the temperature range $80<T<400$ K using the 3ω method.[13,111] HSQ is a spin-on material with dielectric permittivities near to 2. Figure 13 shows

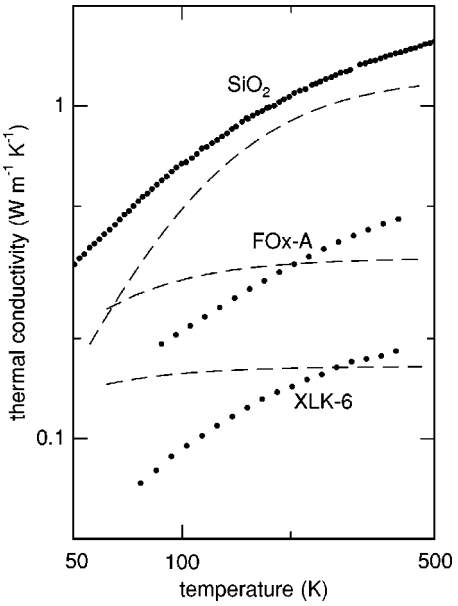

FIG. 13. Comparison of data for hydrogen-silsesquioxane HSQ and SiO_2 (filled circles) to calculations of the minimum thermal conductivity (dashed lines) for each material. The mass density of the "flowable oxide" sample, FOx-*A*, is $\rho = 1.5\ \mathrm{g\,cm^{-3}}$; for the "extra-low-*k*" sample, XLK-6, $\rho = 0.90\ \mathrm{g\,cm^{-3}}$.

the results of thermal conductivity measurements on a variety of HSQ samples that differ primarily by processing conditions, which is expected to modulate the porosity of resultant films. Remarkably, the temperature dependence of the data is nearly identical for all samples, i.e., the conductivity of HSQ is suppressed relative to SiO_2 by a constant factor that is independent of temperature in the temperature range of the experiments, $80 < T < 400$ K, and a significant difference in porosity does not appear to modify the character of thermal transport.

Thus, the nearly identical temperature dependence of the thermal conductivities of SiO_2, FO_x, and XLK suggests that the spectrum of heat-carrying vibrational modes is nearly the same in all three materials. It is thus attractive to conclude that heat transport in these materials is intrinsically local and that porosity does not play a role except to reduce average density. However, this is the basic physical picture of the minimum thermal conductivity theory applied above for the doped oxides.[108] The results of this theory applied to the HSQ materials are presented in Fig. 13, where it is evident that with increasing porosity, there is an increasingly poor match between the data and the model. Effective medium theory (Refs. 112 and 113) in which the porous solid is treated as a composite material of a matrix punctuated by voids offers a path to better understand these materials.[110]

B. Multilayers and superlattices

Multilayers and superlattices are films that contain alternating layers of two different materials stacked upon each other. In multilayers the films may be amorphous or polycrystalline while in superlattices the films are single crystal. In this section, we concentrate on the thermal conductivity in the direction perpendicular to the plane of the film because this is the property accessible to the most commonly used experimental techniques: time-domain thermoreflectance, see Sec. V A, and the 3ω method for thin films.[111,13] (When the width of the heater/thermometer line in the 3ω method is comparable to the film thickness, the 3ω method is also sensitive to the thermal conductivity in the plane of the film.[114] Data collected using combinations of narrow and wide metal lines can be used to separate the in-plane and cross-plane conductivities.[114])

Phonon transport in superlattices and multilayers can be divided into two categories, namely: (i) $\ell < b$; and (ii) $\ell > b$, where ℓ is the phonon mean free path and b is the superlattice period. Consider the first regime. There have been a number of studies of thermal transport in multilayer films[12,14,115] with heat transport perpendicular to the plane of the film. The general conclusion from these studies is that if the thermal conductivity of a thin layer of disordered material is independent of layer thickness b, i.e., if phonons with mean-free-paths comparable to b make a negligible contribution to heat transport, and that the microstructure of the thin layer is approximately independent of b, the measured resistance of a multilayer sample is the series sum of the thermal resistance of the individual layers and the thermal resistance of the interfaces.[13,116] Thus, a simple way of predicting the thermal conductivity is to add up the bulk plus interfacial resistances of all the layers.

Figure 1 shows the data and predictions for the thermal conductance of a single interface. The values range from 3 to 200 $\mathrm{MW\,m^{-2}\,K^{-1}}$ at room temperature while the predictions of the diffuse mismatch model (DMM) tend to be on the order of 500 $\mathrm{MW\,m^{-2}\,K^{-1}}$. While this discrepancy continues to exist, in many cases the interfacial resistance is negligible compared to the bulk resistance of a single layer. This often occurs when the films are amorphous. In such cases, the thermal conductivity of multilayer films is found to be independent of period b. Studies of multilayers of disordered oxides have failed to reveal a significant effect of interfaces: the thermal conductivity of $ZrO_2{:}Y_2O_3/SiO_2$ (Ref. 117) and ZrO_2/Y_2O_3 (Ref. 12) multilayers are almost independent of layer thickness with layer thickness as small as 4 nm. Apparently, the lattice vibrations of these oxides are sufficiently alike that the thermal conductance is too large to be observed by this approach. Multilayer coatings[115] do not, therefore, appear to be a promising route for lowering the conductivity of thermal barriers. Significant decreases in conductivity have been observed recently in nanocrystalline $ZrO_2{:}Y_2O_3$ (Ref. 118) and attributed to the finite thermal conductance of grain boundaries.

Theoretical and experimental studies on thermal transport in epitaxial superlattices have been conducted for more than two decades. In most cases, phonon transport in superlattices fall into the second regime, i.e., $\ell > b$. Hence, both wave and particle-like phonon effects are observed, offering not only richness in physics but also difficulties in predictions. The origins of this work can be traced back to Narayanamurti *et al.*;[119] they studied monochromatic phonon transport across lattice matched GaAs/AlGaAs superlattices and showed the existence of a phonon band gap. This is a coupled behavior resulting from interference of waves re-

TABLE I. Experimental research on thermal transport in semiconductor superlattices. Unless otherwise noted, the comments refer to cross-plane transport. AM stands for ''acoustic mismatch.''

Reference	Materials	Effects considered	Temperature behavior	Period behavior	Lowest thermal conductivity
124	GaAs/AlAs	not applicable	not applicable	in-plane: max at 200 Å	in-plane: 12 $W m^{-1} K^{-1}$
125	GaAs/AlAs	interface roughness	in-plane: decrease 190–450 K	(700 Å/700 Å only)	in-plane: ≈40
133	GaAs/AlAs	AM, band gaps, roughness	decrease 100–400 K	increase 10–400 Å	4
122	Si/Ge	dislocations	increase to ≈150 K	maximum at 70 Å	≈1.6
67	$Si/Si_{0.71}Ge_{0.29}$	AM	not applicable	50 Å/50 Å only)	22, in-plane: 54
123	Si/Ge	doping, period, dislocations	increase 80–150 K, constant to 330 K	decrease $b=40$–90 Å slight decrease to $b=140$ Å	1.2
127	$Si/Si_{0.7}Ge_{0.3}$	AM	increase 100–300 K	increase for $b=45$–300 Å	10
134	$Si_{0.84}Ge_{0.16}/Si_{0.76}Ge_{0.24}$	AM	increase 50–180 K, constant to 300 K	in-plane: max shifts with period constant for $b=67$, 100, 133 Å	8.4
128	InAs/AlSb	growth temp, annealing	maximum at 150 K	not applicable	2.5
135	InP/InGaAs	thickness ratio	increase 50–100 K	not applicable	7
132	Bi_2Te_3/Sb_2Te_3	doping, tunneling, localization	not applicable	lattice: minimum at 40 Å	0.2
12	PbTe/PbSe	not applicable	decrease 200–400 K	40 Å only	1.6

flected from multiple interfaces. For this to occur, the mean free path of phonons must span multiple interfaces (>10). In this regime, the phonon dispersion relation is modified and zone folding occurs resulting in multiple phonon band gaps.[120] Several effects can result from this modification of the phonon dispersion. First, the group velocities of phonons are reduced significantly, especially for higher energy acoustic phonons. Second, because $\omega-k$ relations are modified, there are many more possibilities for conservation of crystal momentum and energy involved in normal and umklapp scattering.[121] Hence, the scattering rate is increased.

In the regime when the mean free path is not large enough for phonon band gaps to occur, single interface effects can also play a significant role. For example, if the two materials in the superlattice have large mismatch in the phonon dispersion relations, phonons in certain frequency range cannot propagate to the neighboring layer unless there are mode conversions at the interface. In addition to these effects, interfaces between two different materials with different lattice constants can contain dislocations and defects. These can also scatter phonons and reduce thermal conductivity. Finally, depending on the type of processing, there could be both physical roughness as well as alloying at the interface, which can also influence phonon transport. Hence, it is clear that there are many different effects that contribute to the resistance to heat flow.

To dissect the contributions of these effects, several experimental and theoretical studies have been performed. Table I lists the experimental work done in this area while Table II lists the theoretical and computational ones. Most experimental studies have used superlattices of Si, Ge, and their alloys as well as those of III–V. Table I also shows the

TABLE II. Theoretical research on thermal transport in semiconductor superlattices. AM stands for ''acoustic mismatch.''

Reference	Superlattice	Model	Effects considered	Comparison with experiment
121	general	phenomenological	minibands	conductivity increases with period
136	Si/Ge	sc lattice dynamics	AM, phonon confinement, minibands	room temperature reduction agrees well with Si/Ge
137–139	Si/Ge; GaAs/AlAs	Boltzmann transport equation	AM, inelastic scattering, roughness	see references
140	Si/Ge	fcc lattice dynamics	minibands, velocity	trend does not agree with experimental results
141	general	transfer matrix	phonon interference, tunneling	poor agreement with experiment
142	GaAs/AlAs	lattice dynamics	velocity reduction	poor agreement with experiment
143	Si/Ge	valence-force potential	velocity reduction, spectra mismatch	periods too thin for comparison
144	Si/Ge & GaAs/AlAs	fcc lattice dynamics	minibands, tunneling	good agreement for cross-plane; poor agreement in-plane
120	general	wave theory	mini-bands, interface scattering	trend agrees with lattice conductivity of Bi_2Te_3/Sb_2Te_3
145	Si/Ge	molecular dynamics	all classical effects	good agreement (two points) with experiment
146	general	phenomenological	particle-wave crossover	high TC at ultra-short periods; model cannot explain trend
147	SiGe quantum dot	continuum	quantum dot scattering	not applicable
132	Bi_2Te_3/Sb_2Te_3	Boltzmann transport equation	AM, interface roughness, localization	trend does not agree with data
148	Lennard–Jones solids	molecular dynamics	all classical effects, strain	not applicable
149	fcc	molecular dynamics	all classical effects	not applicable

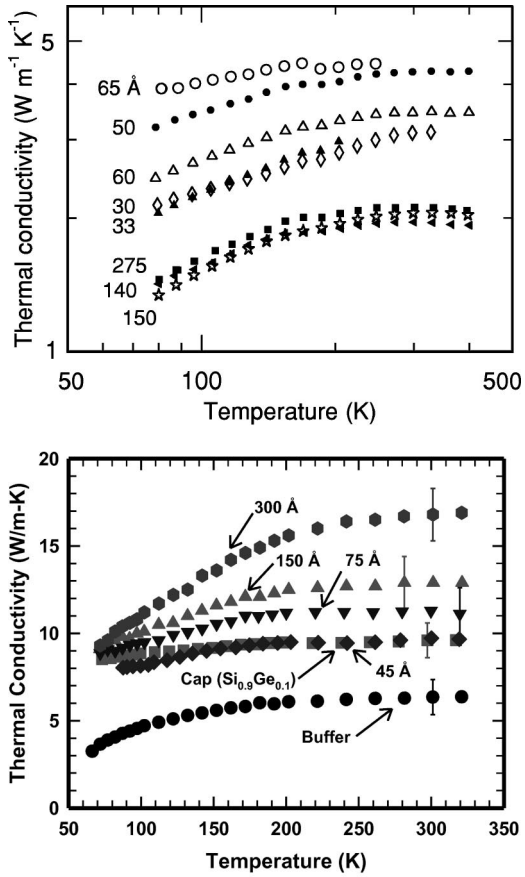

FIG. 14. Thermal conductivity of Si/Ge (top) (Ref. 122) and $Si/Si_{0.7}Ge_{0.3}$ (bottom) (Ref. 127) superlattices; the curves are labeled by the superlattice period in Å. The thermal conductivity of Si/Ge superlattices (top) increases with period thickness in the region of 30–60 Å, but then drops dramatically for period higher than 140 Å, presumably due to presence of misfit dislocations and defects beyond a critical thickness. The thermal conductivity of $Si/Si_{0.7}Ge_{0.3}$ with thickness ratio of 2:1 showed that as the period was decreased from 300 Å (100 periods in 3 μm thick film) to 45 Å (667 periods in 3 μm thick film), the thermal conductivity decreased steadily and approached the effective alloy which is $Si_{0.9}Ge_{0.1}$.

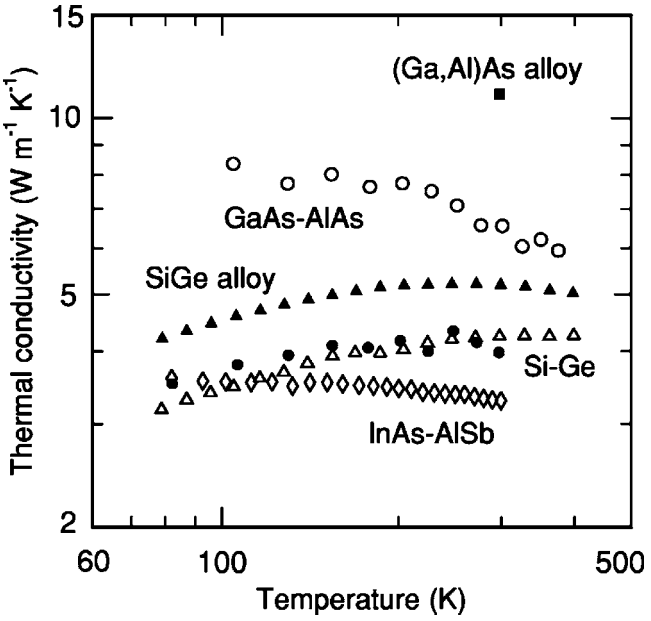

FIG. 15. Selected data for the through-thickness thermal conductivity of superlattices with bilayer periods of $\approx$5 nm; data for GaAs–AlAs [open circles, 5.67 nm period (Ref. 126)] were measured by picosecond thermoreflectance; data for Si–Ge [open triangles, 5 nm period (Ref. 122); filled circles, 4.4 nm period (Ref. 123)] and InAs–AlSb [open diamonds, 6.5 nm period (Ref. 128) were measured using the 3ω method. Data for $Si_{0.85}Ge_{0.15}$ (Ref. 122) and $Ga_{0.4}Al_{0.6}As$ (Ref. 129) alloys are included for comparison.

effects considered (interfacial roughness, phonon band gaps, dispersion mismatch, etc.) and the observed dependence of thermal conductivity on temperature and superlattice period. The data on Si and Ge superlattices suggest that for very small period, when the layer thickness is less than the critical one for the extension of misfit disclocations, the thermal conductivity of superlattices tend to decrease with decreasing layer thickness.[122] As the layer thickness is increased beyond 10 nm, the thermal conductivity drops, presumably due to disorder created by extensive plastic deformation [see Fig. 14(a)]. This is similar to the observations of BorcaTascuic *et al.*[123]

Interface disorder introduces diffuse scattering but interface disorder in a superlattice is typically modest. It is limited to interface roughness (a finite density of interface steps) and substitutional alloying at the interfaces caused by surface segregation during growth. Unfortunately, this physical and chemical interface roughness in an epitaxial superlattice is sensitive to the material, growth method, growth temperature, and deposition rate—and is notoriously difficult to characterize. Furthermore, asymmetry of the interface is often pronounced, i.e., the growth of component *A* on the surface of component *B* creates a different interface than the growth of *B* on *A*. Strained-layer superlattices such as Si–Ge can harbor high densities of crystalline defects when the layer thickness exceeds the critical thickness for the extension of misfit dislocations; growth on relaxed buffer layers reduces the density of threading dislocations but the misfit density will still be large when the critical thickness is exceeded. The agreement between the data of Cahill *et al.*[122] and BorcaTascuic *et al.*[123] seem to support this idea. The interesting observation that they both made was that the superlattice thermal conductivity was lower than that of the alloy with the same mass ratios (see Fig. 15). Hence, interface scattering alone is probably insufficient to explain this observation. Perhaps this may be due to zone folding which reduces phonon group velocities and increases scattering rates and thereby reduces thermal conductivity. Thermal transport in GaAs and AlAs superlattices have also been studied widely.[66,124–126] These studies have shown that as the interface density increases, the thermal conductivity decreases, clearly showing that interface resistance is important.

More recently, Huxtable *et al.*[127] have shown that for superlattices of Si and $Si_{0.7}Ge_{0.3}$, where the critical thickness is much larger than that for Si and Ge superlattices, the thermal conductivity scaled almost linearly with interface density supporting the data of Cahill *et al.*[122] and BorcaTascuic[123] [see Fig. 14(b)]. As the interface density increased, the thermal conductivity approached that of the alloy, but was never lower than that of the alloy, which is in contrast with previous observations. Clearly, the mismatch in acoustic impedance between Si and Ge is more than that of

Si and $Si_{0.7}Ge_{0.3}$. Hence, it is possible that thermal conductivities below alloy values can be found only when there is large mismatch in acoustic impedance that creates significant band gaps in the phonon dispersion relation.

There have been two reports of thermal conductivity of Bi_2Te_3 and Sb_2Te_3 superlattices. These are of interest in thermoelectric applications where the reduction of thermal conductivity has been a major challenge.[130] Venkatasubramanian[131] showed as the period thickness increased, the room temperature thermal conductivity reached a minimum for a period thickness 5 nm, and this value was lower than the thermal conductivity of the corresponding alloy. It was suggested that this was due to phonon band-gap effects. However, Touzelbaev *et al.*[132] did not find any significant change in thermal conductivity when the superlattice period was varied. Hence, it remains inconclusive as to whether phonon band-gap effects are indeed present in this system.

Table II lists the theoretical and computational work on thermal transport in superlattices. Three approaches are generally adopted. The first is based on wave propagation, the second on particle transport that can be modeled by Boltzmann transport theory, and the third relies on molecular dynamics.

From the experimental and theoretical studies, it is clear that the mechanism of phonon transport in epitaxial superlattices is not well understood and it is difficult to predict the value of thermal conductivity. However, a few trends do seem to appear. First, if interface resistance is to play a major role, the acoustic mismatch between the two films of the superlattice must be sufficiently large, >1.1. For incoherent phonons, acoustic mismatch gives rise to interface reflection while for coherent phonons, phonon band gaps are formed that reduce the group velocities. Second, interface roughness and alloying can also scatter phonons and thereby increase interfacial resistance. Third, in some cases, the phonon thermal conductivity can be reduced below the alloy limit, which may occur due to band-gap formation. Although calculations predict this, experiments have not provided unmistakable proof. The image that seems to emerge from all these studies is the following. To reach the minimum thermal conductivity, one perhaps needs to take different approaches to block phonon transport in different parts of the phonon spectrum. For example, high-frequency phonons can be blocked by alloy scattering since the wavelengths are generally on the order of a few atomic spacings. Low frequency phonons are generally unaffected by alloy scattering since the scattering is generally in the Rayleigh regime. However, they may dominate energy transport in an alloy. For such phonons, superlattice formation would lead to miniband formation since their mean free paths are generally much larger than for high-frequency phonons. Hence, what would indeed be interesting is to study thermal transport in superlattices of alloys that have sufficient acoustic impedance mismatch.

C. Superlattices: Theory and computation

Thermal transport in semiconductor superlattices can be either parallel or perpendicular to the plane of the layers. The initial measurements and theories were for transport parallel to the layers. The simple viewpoint is that heat transport should be quite efficient parallel to the layers. If the interfaces are atomically smooth, then phonons would specularly reflect from these interfaces. Each layer becomes a phonon waveguide which efficiently channels heat along each layer. The initial measurements of thermal conductivity parallel to the layers found values smaller than bulk values by a factor of four. Yao[124] found in GaAs/AlAs superlattices that the thermal conductivity was similar to that of a random alloy of the two materials. This was explained in Ref. 150 as due to the interface boundaries not being perfectly planar. Atomic scale defects at the interface are efficient scattering centers for the phonons.

There is much more interest in thermal transport perpendicular to the plane of the layers, which is called the ''cross-plane'' direction. In some cases experiments show a thermal conductivity significantly lower than that of the random alloy of the two materials in the superlattice.[122,131,133] The simple explanation for this reduction is that the superlattice acts as a Fabrey–Perot interferometer, and allows only a few phonon frequencies to pass through. This feature was demonstrated by phonon transmission spectroscopy.[119]

There have been many calculations of thermal conductivity in the cross plane direction. They can be divided into three groups. The largest number of calculations are based on the standard formula for the thermal conductivity

$$\kappa=\hbar\sum_{\lambda}\int\frac{d^3q}{(2\pi)^3}v_{z\lambda}(\mathbf{q})^2\omega_{\lambda}(\mathbf{q})\tau_{\lambda}(\mathbf{q})\left(\frac{dn_B[\omega_{\lambda}(\mathbf{q})]}{dT}\right), \tag{8}$$

where $v_{z\lambda}(\mathbf{q})$ is the velocity of the phonon, $\tau_{\lambda}(\mathbf{q})$ is the lifetime, and $n_B[\omega_{\lambda}(\mathbf{q})]$ is the Boson occupation function. The above formula is derived from the Boltzmann transport equation (BTE). Calculation by Kato et al,[151] Hyldgaard and Mahan,[136] Tamura *et al.*,[140] Simkin and Mahan,[120] Bies *et al.*,[142] and Kiselev *et al.*,[143] all just calculate the actual phonon modes of the superlattice and evaluate the above formula. Usually the lifetime $\tau_{\lambda}(\mathbf{q})$, or else the mean-free-path $\ell_{\lambda\mathbf{q}}$ is selected to be the same as in the homogeneous material. These calculations show the thermal conductivity in the superlattice is reduced significantly, sometimes by a factor of ten, compared to that of the constituents of the superlattice. This large reduction agrees with the experimental findings.

Simkin and Mahan[120] used a complex wave vector in computing the superlattice modes. The imaginary part of the wave vector was a phenomenological way of including the mean-free-path into the calculation of the phonon modes. This calculation showed a minimum in the thermal conductivity as a function of superlattice period.

There have been several calculations of the thermal conductivity of the superlattice which have solved the Boltzmann transport equation. That of Ren and Dow[121] did not predict a large reduction of the thermal conductivity, and disagrees with experiments. Several calculations from Chen's group[138,152] agree much better with experiment.

Recently, Daly and co-workers[149,153] used large-scale (1.3×10^6 atoms) molecular dynamics simulations to calcu-

late the thermal conductivity of superlattices.

There have been very few calculations of thermal conductivity in the cross plane direction which included heat transfer by electrons as well as phonons. Bartkowiak and Mahan's modeling[146] was semiclassical and assumed that both the electrons $T_e(x)$ and phonons $T_p(x)$ had a local temperature. The electrons and phonons can exchange energy in the bulk, and at the interfaces. They found a wide variety of temperature distributions depending upon the various boundary resistances for electrons and phonons. None of this behavior has been verified or refuted by experimental measurements. All of their calculations depend on the concept of a local temperature.

V. NEEDS AND LIMITS OF METROLOGY

The goal of successful commercial implementation of nanoscale materials places a burden on the metrology of these materials and devices that extend beyond the characterization of the fundamental materials properties. This burden involves not only the small physical dimension of the material but also the general accuracy of the measurement. To illustrate this, perhaps the most familiar examples derive from the Si semiconductor industry. Here, thin film metrology is becoming increasingly challenging as Si semiconductor device technology scales toward smaller dimensions and the corresponding manufacturing process complexity grows. Traditional thin film properties such as thickness and intrinsic stress are being augmented by an increasing number of other physical parameters, which together must be considered in the development and manufacturing monitoring plan. Such parameters include density, porosity, thermal conductivity, grain texture, surface chemical residue, and bulk and interface cohesion. The introduction of more complex devices using new materials and process methods (e.g., Si alloys, polymers, and 3D structures) also contribute to the measurement challenge. Effective control of these properties often becomes difficult as the device scaling continues. For example, the control of the physical thickness and composition profile of the MOS gate dielectric is generally of critical importance to the resultant device parameters. But with this film currently having a required thickness of less than 1 nm, the challenge is to control thickness and composition variation on the atomic scale.

Another factor to consider is that the ability to measure many properties is becoming less and less feasible at the nanoscale limit. A well known example is the measurement of dopant distributions under a gate as the gate widths move below the 50 nm scale and approach the ''sparse dopant'' limit.[154] As a result, an increasing number of traditional measurement methods are becoming insensitive or unsuitable for use due to the limitations of the physics employed. To address these difficulties, not only is new instrumentation being sought, but also industry is relying increasingly on materials, device, and thermal-mechanical modeling to infer properties that cannot be directly measured. This approach, in turn, requires that the fundamental properties be precisely and accurately measured on test systems, designed to enable such measurements.

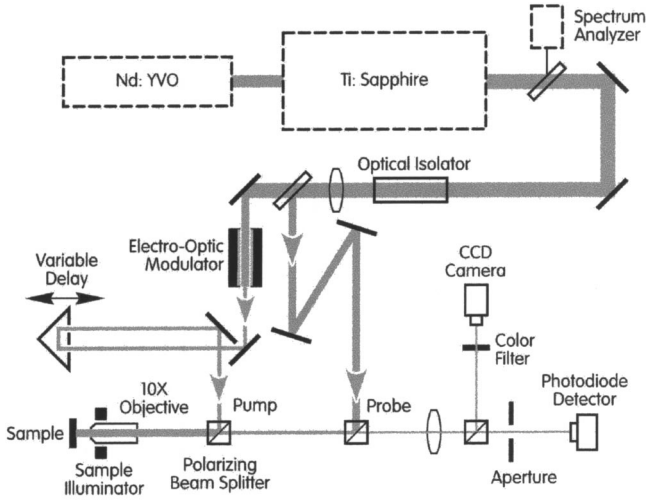

FIG. 16. Schematic of the TDTR and picosecond acoustics apparatus in use at the Laser Facility of the Frederick Seitz Materials Research Laboratory.

The consequence of the above considerations for the problem of heat transport in nanostructures has been the introduction of a wide variety of novel instrumentation well suited for measurement of thin films and structures. Several promising approaches have been introduced recently or are currently under development. Three examples are described below.

A. Time-domain thermoreflectance

The first thermal transport experiments using picosecond thermoreflectance, alternatively referred to as time-domain thermoreflectance (TDTR), were reported in Refs. 155 and 156. TDTR provides a direct method for measuring heat diffusion on nanometer length scales. Most engineering materials have thermal diffusivities D in the range $0.005 < D < 1\ \mathrm{cm^2\,s^{-1}}$ and at $t = 200$ ps, heat diffusion lengths $l = \sqrt{Dt}$ are in the range $10 < l < 140$ nm. Therefore, picosecond time resolution offers nanometer-scale depth resolution and, more specifically, picosecond thermoreflectance can isolate the effects of interface conductance from the thermal conductivity of a thin layer. By contrast, thermoreflectance measurements using longer pulse length Q-switched lasers[157] and the 3ω method[13] cannot distinguish between the thermal conductivity of a film and the thermal conductance of its interfaces.

An example of TDTR experimental apparatus is presented in Fig. 16. Picosecond time resolution is obtained using mode-locked lasers that produce a series of <1 ps pulses at a repetition rate of ≈ 76 MHz. Extremely high time resolution is achieved by splitting the laser output into two beam paths, a ''pump'' beam and a ''probe'' beam, and adjusting the relative optical path lengths with a mechanical delay stage. If the sample under investigation is metallic, or can be coated with a thin metal film, then a small fraction of the energy from each pulse in the pump beam produces a sudden jump in temperature of ~ 3 K near the surface of the sample. The decay of the near-surface temperature is then interrogated by the reflected energy of the series of pulses in the probe beam. Determination of the thermal conductivity

and interfacial thermal resistance is made by comparing the experimental cooling curve to the theoretical model and optimizing the free parameters. For all but the shortest times, the temperature is homogeneous through the optical absorption depth of the thin metal film and $\Delta R_1(t) = (dR/dT)\Delta T_1(t)$. The surface temperature $\Delta T_1(t)$ can be accurately calculated using one-dimensional heat flow since the thermal diffusion length is usually much smaller than the radius of the focused pump beam.[133]

In a modulated pump–probe experiment, the differences in reflected probe intensity caused by the pump pulse appear at the modulation frequency of the pump beam and are extracted with lock-in detection but interpretation of this lock-in signal is not straightforward as the time delay becomes a significant fraction of the separation between pulses: Capinski and co-workers[133] discuss calculations of the in-phase and out-of-phase signals of the lock-in amplifier given the time-domain thermal response of the sample; Cahill *et al.*[1] provide a calculation starting from the frequency-domain response.

Despite the promise of these methods, few quantitative and systematic studies of thermal properties of materials have used picosecond optical techniques.[10,11,133,156,158,159] Experiments by Maris and co-workers on interface thermal conductance[10] and superlattice conductivity[133] are the most complete. Data for the thermal decay at short times $t < 50$ ps are difficult to interpret quantitatively because (i) hot-electrons can deposit energy beyond the optical absorption depth, (ii) the temperature dependence of the complex index of refraction $d\tilde{n}/dT$ is typically unknown, (iii) the diffusion equation fails on length scales comparable to the mean-free-paths of the dominant energy carriers, and (iv) the assumption of equilibrium between phonons and electrons is not always valid. At long times $t > 500$ ps, measurements are often plagued by shifts in the focal plane and beam overlap created by large displacements of the delay stage. (Capinski and Maris[104] describe an optical design that improves accuracy at long delay times; the out-of-phase signal of the lock-in amplifier can also be used to correct systematic errors.[1]) It is likely, however, that improved performance and dropping costs of solid-state mode-locked lasers will expand applications of picosecond thermoreflectance. Reliable, low-noise Ti:sapphire lasers that produce 100 fs pulses are commercially available and can be operated with only a modest knowledge of the technology of ultrafast lasers.

Over the longer term, improved laser performance will also make more sophisticated experiments possible. For example, the pump and probe light pulses can be applied to localized regions of the sample through the use of near field optics. With this technique, it should be possible to study the lateral flow of heat in a thin film, instead of just the flow of heat through the film. In addition, the accuracy of TDTR measurements will be enormously enhanced if compact laser sources that can be tuned over a wide wavelength range become available. The probe wavelength could then be chosen to match a peak in the thermoreflectance of the metal film. This would increase signal to noise in the measurement process, reduce the time needed for a measurement, and improve the accuracy.

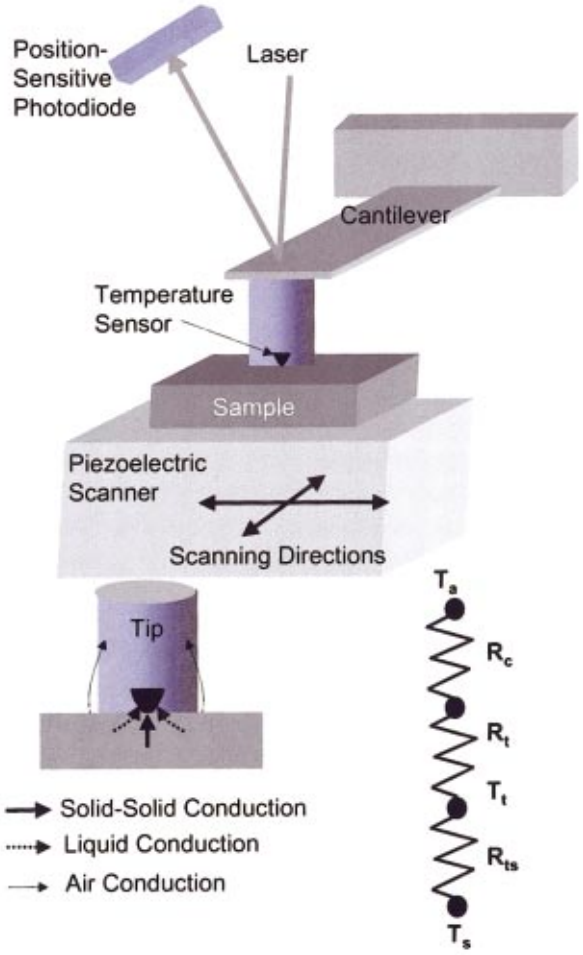

FIG. 17. (Color) Schematic diagram of a scanning thermal microscope (SThM). It consists of a sharp temperature-sensing tip mounted on a cantilever probe. The sample is scanned in the lateral directions while the cantilever deflections are monitored using a laser beam-deflection technique. Topographical and thermal images can be thermally obtained. The thermal transport at the tip-sample contacts consists of air, liquid, and solid–solid conduction pathways. A simple thermal resistance network model of the sample and probe combination, shows that when the sample is at temperature T_s, the tip temperature T_t depends on the values of the thermal resistances of the tip-sample contact, R_{ts}, the tip, R_t, and the cantilever probe, R_c.

B. Microfabricated probes

Access to nanofabrication facilities offers new opportunities for probing directly the local temperature and thermal transport mechanisms in nanostructures. Two significant approaches will be commented on below: scanning thermal microscopy and the new area of microinstrumentation fabrication.

A scanning thermal microscope (SThM) operates by bringing a sharp temperature-sensing tip in close proximity to a sample solid surface (see Fig. 17). Localized heat transfer between the tip and sample surface changes the tip temperature. By scanning the tip across the sample surface, a spatial map of the tip-sample heat transfer is mapped out. When the tip comes in local equilibrium with the sample, one obtains the spatial temperature distribution of the sample surface, whereas if the temperature change is determined for a known heat flux, one could obtain the local thermal prop-

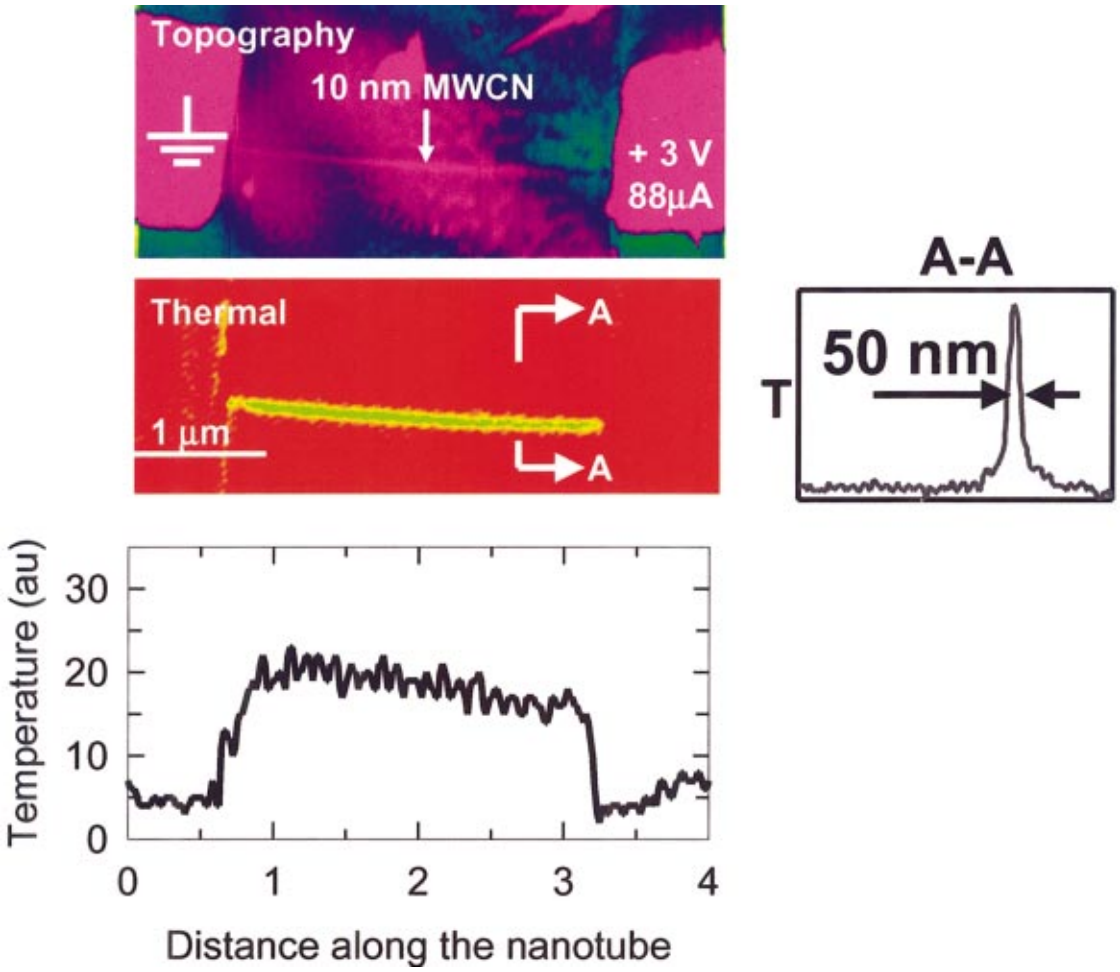

FIG. 18. (Color) Topographical (top) and thermal images of a multiwall carbon nanotube (MWCN), 10 nm in diameter obtained by SThM. The bottom plot shows the temperature distribution along the length of the wire while the plot on the side shows the cross-sectional temperature profile, indicating full-width half maximum of the temperature peak to be 50 nm.

erties. The spatial resolution depends mainly on three factors, namely, tip sharpness, tip-sample heat transfer mechanism, and the thermal design of the probe. In the recent past, the spatial resolution has been improved to 30–50 nm, allowing one to study thermal transport phenomena at these length scales.[160]

The idea of SThM was first proposed by Williams and Wickramasinghe[161] when they used a thermocouple at the end of a metallic wire to measure temperature. Tip-sample heat transfer was used to image the surface topography of electrically insulating materials. Since then, significant progress has been made in improving thermocouple-based measurements while other techniques based on contact potential, electrical resistance, and thermal expansion have also been developed, which are reviewed in detail by Majumdar.[162] Most of the development has focused on cantilever-based probes such that atomic force microscopes (AFMs)[163] could be used as a platform for SThM. When a temperature sensor is mounted on the very apex of the tip, such probes can be used to image both the topography and the temperature distribution of devices such as single transistors[26,77] and vertical cavity lasers.[164] Such studies have helped in identifying defects and failure mechanisms while providing insight about electron, photon and phonon transport in these devices. In addition, SThM has also been used to measure thermal properties of materials and perform calorimetry at nanometer scales.[165]

There are three important elements determining the performance of SThM, namely: (i) thermal and mechanical design of the probe; (ii) fabrication of probe; (iii) understanding of tip-sample heat transfer. Proper thermal design ensures not only temperature measurement accuracy but also higher spatial resolution.[166,167] Fabrication of probes by MEMS processes allows one to batch fabricate hundreds of probes on a single wafer using optical lithography, enabling multiple users to utilize such probes.[160,166] Recent studies have revealed the role of gas conduction, solid–solid conduction, and conduction through a liquid film bridging the tip and the sample.[164,167] A fundamental understanding of the tip-sample heat transfer allows accurate estimation of sample temperature distributions from the measured data. Recent progress in these areas has allowed thermal imaging of nanostructures such as carbon nanotubes[160] with 30–50 nm spatial resolution (see Fig. 18). Such a high spatial resolution allows one to study phonon physics at the length scale of phonon wavelengths and mean free paths, which could lead to greater understanding of nanoscale thermal transport. In addition, the spatial resolution is sufficiently high to study electrother-

mal and photothermal effects in modern electronic and optoelectronic devices.

Despite these recent advances, there are several unanswered questions that need to be resolved. It is well known that the liquid film bridging the tip and the sample contributes significantly to tip-sample heat transfer. Can the effect of liquid conduction be controlled by tailoring the surface chemistry? What is the role of near-field radiation in tip-sample heat transfer, especially in a vacuum environment? How do phonons and electrons propagate through a point contact that is on the order of their wavelength? Can we conduct SThM experiments at low temperature and observe quantum transport effects? Because tip-sample thermal resistance depends on surface topography, topography-related artifacts in thermal images still remains a problem. There are two potential solutions: a thorough knowledge of tip-sample heat transfer in order to model the effect of topography; or a null-point measurement such that tip-sample temperature difference can be minimized thereby eliminating any heat flow. The latter requires more sophisticated probes with multiple sensors and feedback control. Future progress will be driven towards multiple sensors and actuators on integrated cantilever probes such that one could simultaneously measure temperature and heat flux as well as electrical, optical, and other nanoscale properties while imaging a nanostructure.

Finally, because new nanoscale materials and energy conversion devices are being developed, there will also remain a need to thermally probe them at nanoscales. For example, thermoelectric properties of nanostructured semiconductors are markedly different than those of bulk materials. By simultaneously measuring thermal, electrical, and thermoelectric properties using a multifunctional SThM, one could characterize low-dimensional nanostructures. An area of research that is largely unexplored is SThM under liquid environment, in particular, of biological molecules. Proteins and DNA undergo structural changes and phase transitions at different temperatures. Localized calorimetry of molecules could shed light on the binding behavior of biomolecules.

One of the major limitations of scanning probe microscopes is their inability to probe below a solid surface. Ballistic electron emission microscopy (BEEM) allows one to probe about 10-50 nm below a conducting or a semiconducting surface by detecting electrons that travel ballistically through the material.[168] However, an insulating surface cannot be probed by this technique. Because thermal transport occurs in all materials, it may be possible to use SThM to probe materials below the surface using either ballistic or diffusive phonon transport. While diffusive phonon transport has been explored,[165] ballistic phonon transport has not yet been studied using SThM. A combination of picosecond ultrasonics and SThM might perhaps be able to map out materials and their properties in three dimensions.

The SThM probe falls under a general class of microinstruments that allows one to thermally probe at a length scale that is an order of magnitude smaller than the characteristic dimension of the instrument. By using traditional MEMS fabrication techniques, which allow one to make devices and structures down to about 300 nm, one could study transport phenomena at length scales on the order of 10–50 nm.

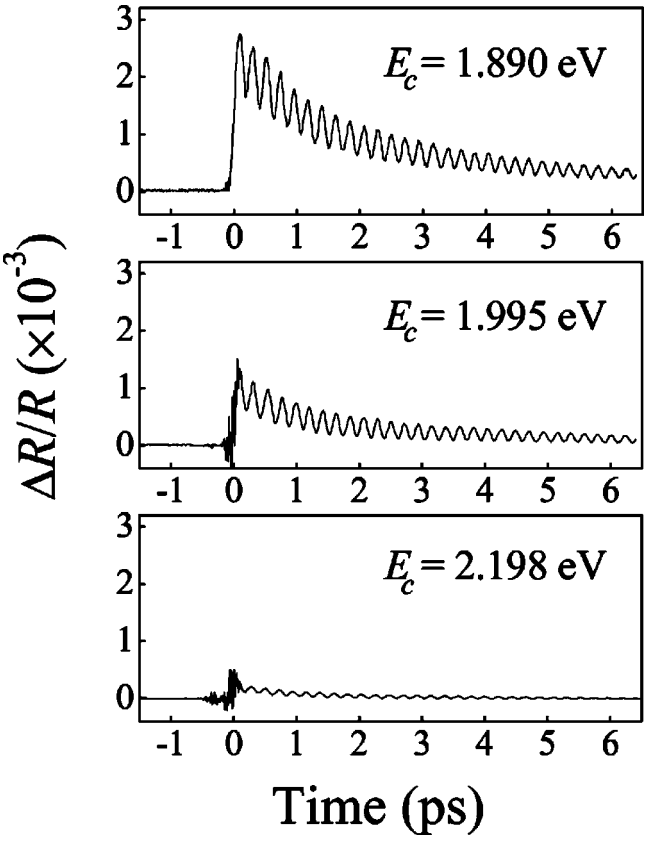

FIG. 19. Normalized differential reflectivity for antimony at 300 K (see Ref. 170). E_c is the central energy of the pulses which are polarized perpendicular to the trigonal axis. The data show coherent A_{1g} phonon oscillations of frequency $\Omega_0 \sim 4.5$ THz and a slowly varying electronic background. The fine structure near zero delay is due to interference between overlapping pump and probe beams.

Hence, MEMS provides a platform to integrate nanostructures and thereby forms a bridge between nano- and microscales. In the case of the SThM probe, the nanoscale tip is integrated onto the rest of the cantilever and the probe. Figure 8 shows another example where two suspended microheaters are fabricated on a chip using standard MEMS techniques.[94] A carbon nanotube or any 1D nanostructure can be placed across the two heater islands and its thermal properties can be measured using this device. An advantage offered by MEMS is that hundreds of microinstruments can be built on a single wafer, providing low cost measuring devices and high-throughput experimentation.

C. Coherent optical methods

Coherent optical methods, such as stimulated Raman scattering, have long been applied to measurements of the lifetime of optical phonons.[169] As illustrated in Fig. 19, laser excitation can lead to the generation of intense vibrations showing a high degree of temporal and spatial coherence.[170] Transport measurements using optically generated coherent phonons, particularly acoustic modes, may provide an alternative to conventional thermal methods for the determination of the mean free path. Coherent, monochromatic phonon beams can be generated using a variety of techniques that combine optical cw or pulsed lasers and a suitable

transducer.[170–173] Laser-induced cw thermomodulation of a thin metallic film gives a tunable source of longitudinally polarized phonons in the 1–5 GHz range.[171] Higher frequencies, up to ~0.5 THz, can be attained using ultrafast (subpicosecond) laser excitation of a layered structure.[172] In semiconductor superlattices, the mechanism for light-sound coupling is the acousto-optic effect, and phase matching is provided by the wave vectors involved in the Fourier decomposition of the structure.[170]

As discussed earlier, it is possible to generate coherent (but not monochromatic) sound pulses as short as 100 Å using picosecond ultrasonic methods. This technique has been recently applied to studies of the phonon dispersion,[173] and measurements of the phonon attenuation could be used to determine the mean free path. We note that coherent phonon sources can potentially be used for microscopy purposes. Here, there is considerable room for improving the resolution. While the wavelengths of propagating modes in solids are small enough to resolve objects separated by, say, 100 Å, the length scale for state-of-the-art ultrasound and tomography methods is 2–3 orders of magnitude larger.[174]

VI. OUTLOOK

The many unresolved fundamental issues; continuing advances in theory, computation, and experimental techniques; and important applications in modern device materials ensure that nanoscale thermal transport will remain a vigorous field of investigation for many years to come. We discuss specific examples of outstanding questions and recommendations for future directions throughout this review but provide a brief summary of some selected examples here.

The limited range of the data for the thermal conductance of solid–solid interfaces is not well understood—theory predicts a much stronger dependence on acoustic mismatch than what is observed. Transport and coherent phonon experiments on individual and superlattice interfaces with systematically controlled and well-characterized structure are needed. A simple, analytical model that captures the basic features of the frequency dependence in the phonon transmission coefficient would be of great use. Large-scale molecular dynamics should be used to evaluate the sensitivity of the thermal conductance to the structural and chemical disorder of the interface. A long term goal is to include electronic and quantum mechanical effects in atomic-level simulations of thermal transport.

Another important long term challenge is the development of techniques that incorporate scattering rates calculated by atomic-level simulations into higher-level approaches, e.g., Monte Carlo solutions of the classical or quantum Boltzmann transport equation. Improvements in scanning thermal microscopy and other nanoscale metrology methods are needed to make quantitative comparisons between experimental observations of nanoscale transport and the predictions of theory.

ACKNOWLEDGMENTS

This report was sponsored by the Council of Material Science and Engineering of the U.S. Department of Energy. The authors thank Dr. Iran Thomas and Professor Peter Flynn for their support. D.G.C. was supported by NSF Grant No. CTS 99-78822 and the U.S. Department of Energy DE-FG02-01ER45938. A.M. greatly appreciates the support of the NSF, the DOE (Engineering Division, Basic Energy Sciences), and DARPA and acknowledges the many contributions of former and current students and post-docs that have contributed in his group, in particular, A. Abramson and S. Huxtable for gathering some of the material for this monograph. He also thanks P. McEuen and his group for their help with nanotube research. H.J.M. was supported by the Air Force Office of Scientific Research MURI Grant entitled Phonon Enhancement of Electronic and Optoelectronic Devices (Grant No. F4962-00-1-0331). R.M. was supported by the National Science Foundation under Grant No. DMR-9876862 and by the Air Force Office of Scientific Research under Contract No. F49620-00-1-0328 through the MURI Program. S.R.P. is pleased to acknowledge the important contributions of P. K. Schelling to this work. He also gratefully acknowledges useful discussions with P. Keblinski and J. A. Eastman. S.R.P. was supported by the U.S. Department of Energy, Office of Science under Contact No. W-31-109-ENG-38.

[1] D. G. Cahill, K. E. Goodson, and A. Majumdar, J. Heat Transfer **124**, 223 (2002).
[2] I. M. Khalatnikov, Sov. Phys. JETP **22**, 687 (1952).
[3] E. T. Swartz and R. O. Pohl, Rev. Mod. Phys. **61**, 605 (1989).
[4] P. L. Kapitza, J. Phys. (Moscow) **4**, 181 (1941).
[5] L. J. Challis, K. Dransfeld, and J. Wilks, Proc. R. Soc. London, Ser. A **260**, 31 (1961).
[6] J. Weber, W. Sandmann, W. Dietsche, and H. Kinder, Phys. Rev. Lett. **40**, 1469 (1978).
[7] J. R. Olson and R. O. Pohl, J. Low Temp. Phys. **94**, 539 (1994).
[8] H. Kinder and K. Weiss, J. Phys.: Condens. Matter **5**, 2063 (1993).
[9] T. Nakayama, in *Progress in Low Temperature Physics*, edited by D. F. Brewer (North-Holland, Amsterdam, 1989), p. 115.
[10] R. J. Stoner and H. J. Maris, Phys. Rev. B **48**, 16373 (1993).
[11] A. N. Smith, J. L. Hostetler, and P. M. Norris, Microscale Thermophys. Eng. **4**, 51 (2000).
[12] D. G. Cahill, A. Bullen, and S.-M. Lee, High Temp.-High Press. **32**, 135 (2000).
[13] S.-M. Lee and D. G. Cahill, J. Appl. Phys. **81**, 2590 (1997).
[14] E.-K. Kim, S.-I. Kwun, S.-M. Lee, H. Seo, and J.-G. Yoon, Appl. Phys. Lett. **76**, 3864 (2000).
[15] K. H. Wichert, C. Reimann, G. Blahusch, and H. Kinder, Ann. Phys. **4**, 175 (1995).
[16] J. P. Wolfe, *Imaging Phonons* (Cambridge University Press, Cambridge, 1998).
[17] M. Msall, W. Dietsche, K. J. Friedland, and Q. Y. Tong, Phys. Rev. Lett. **85**, 598 (2000).
[18] H.-Y. Hao, D. K. Sadana, and H. J. Maris, Electrochem. Solid-State Lett. **1**, 54 (1998).
[19] H. T. Grahn, H. J. Maris, and J. Tauc, IEEE J. Quantum Electron. **25**, 2562 (1989).
[20] C. J. K. Richardson, M. J. Ehrlich, and J. W. Wagner, J. Appl. Phys. **85**, 861 (1999).
[21] A. Bartels, T. Dekorsy, H. Kurz, and K. Köhler, Appl. Phys. Lett. **72**, 2844 (1998).
[22] C. K. Sun, J. C. Liang, C. J. Stanton, A. Abare, L. Coldren, and S. DenBaars, Appl. Phys. Lett. **75**, 1249 (1999).
[23] Ü. Özgür, C.-W. Lee, and H. O. Everitt, Phys. Rev. Lett. **86**, 5604 (2001).
[24] H. S. Carslaw and J. C. Jaeger, in *Conduction of Heat in Solids* (Oxford University Press, New York, 1959), pp. 109–112.
[25] J. M. Ziman, *Electrons and Phonons* (Clarendon, Oxford, 1960).
[26] A. Majumdar, J. Heat Transfer **115**, 7 (1993).
[27] P. B. Allen and J. L. Feldman, Phys. Rev. B **48**, 12581 (1993).

[28] D. C. Rapaport, *The Art of Molecular Dynamics Simulation* (Cambridge University Press, Cambridge, 1995).
[29] P. K. Schelling, S. R. Phillpot, and P. Keblinski, Phys. Rev. B **65**, 144306 (2002).
[30] W. E. Pickett, J. L. Feldman, and J. Deppe, Modell. Simul. Mater. Sci. Eng. **4**, 409 (1996).
[31] A. Maiti, G. D. Mahan, and S. T. Pantelides, Solid State Commun. **102**, 517 (1997).
[32] P. K. Schelling, S. R. Phillpot, and P. Keblinski, Phys. Rev. B **65**, 144306 (2002).
[33] P. Keblinski, S. R. Phillpot, D. Wolf, and H. Gleiter, J. Acoust. Soc. Am. **80**, 717 (1997).
[34] C.-W. Nan, R. Birringer, D. R. Clarke, and H. Gleiter, J. Appl. Phys. **81**, 6692 (1997).
[35] E. H. Kennard, *Kinetic Theory of Gases* (McGraw-Hill, New York, 1938).
[36] W. G. Vincenti and C. H. Kruger, *Introduction to Physical Gas Dynamics* (Krieger, Malabar, FL, 1975).
[37] R. Siegel and J. R. Howell, *Thermal Radiation Heat Transfer* (Hemisphere, New York, 1972).
[38] M. Q. Brewster, *Thermal Radiative Transfer and Properties* (Wiley, New York, 1992).
[39] S. Rosseland, *Theoretical Astrophysics: Atomic Theory and the Analysis of Stellar Atmospheres and Envelopes* (Clarendon, Oxford, 1936).
[40] D. A. Young and H. J. Maris, Phys. Rev. B **40**, 3685 (1989).
[41] G. Fagas, A. G. Kozorezov, C. J. Lambert, and J. K. Wigmore, Physica B **263–264**, 739 (1999).
[42] P. K. Schelling, S. R. Phillpot, and P. Keblinski, Appl. Phys. Lett. **80**, 2484 (2002).
[43] H. B. G. Casimir, Physica **5**, 595 (1938).
[44] C. Oligschleger and J. C. Schön, Phys. Rev. B **59**, 4125 (1999).
[45] B. C. Larson, J. Z. Tischler, and D. M. Mills, J. Mater. Res. **1**, 144 (1986).
[46] M. L. Huberman and A. W. Overhauser, Phys. Rev. B **50**, 2865 (1994).
[47] A. V. Sergeev, Phys. Rev. B **58**, R10199 (1998).
[48] G. D. Mahan, *Many-Particle Physics* (Kluwer-Plenum, Dordrecht, 2000).
[49] W. R. Frensley, Rev. Mod. Phys. **62**, 745 (1990).
[50] J. R. Hellums and W. R. Frensley, Phys. Rev. B **49**, 2904 (1994).
[51] Special issue, IEEE Trans. Electron Devices **45**, (1998).
[52] J. A. Davis, R. Venkatesan, A. Kaloyeros, M. Beylansky, S. J. Souri, K. Banerjee, K. C. Saraswat, A. Rahman, R. Reif, and J. D. Meindl, Proc. IEEE **89**, 305 (2001).
[53] W. P. King, T. W. Kenny, K. E. Goodson, G. Cross, M. Despont, U. Durig, H. Rothuizen, G. K. Binnig, and P. Vettiger, Appl. Phys. Lett. **78**, 1300 (2001).
[54] P. D. Vu, Xiao Liu, and R. O. Pohl, Phys. Rev. B **63**, 125421 (2001).
[55] M. Asheghi, K. Kurabayashi, K. E. Goodson, R. Kasnavi, and J. D. Plummer, in *Proceedings of the 33rd ASME/AIChE National Heat Transfer Conference* (Asme, New York, 1999).
[56] M. Von Arx, O. Paul, and H. Baltes, J. Microelectromech. Syst. **9**, 136 (2000).
[57] S. Uma, A. D. McConnell, M. Asheghi, K. Kurabayashi, and K. E. Goodson, Int. J. Thermophys. **22**, 605 (2001).
[58] A. D. McConnell, U. Srinivasan, M. Asheghi, and K. E. Goodson, J. Microelectromech. Syst. **10**, 360 (2001).
[59] C. J. Glassbrenner and G. A. Slack, Phys. Rev. A **134**, 1058 (1964).
[60] M. Asheghi, M. N. Touzelbaev, K. E. Goodson, Y. K. Leung, and S. S. Wong, J. Heat Transfer **120**, 30 (1998).
[61] M. G. Holland, Phys. Rev. **132**, 2461 (1963).
[62] J. M. Ziman, *Electrons and Phonons* (Oxford University Press, Oxford, 1960).
[63] K. E. Goodson, J. Heat Transfer **118**, 279 (1996).
[64] Y. S. Ju and K. E. Goodson, Appl. Phys. Lett. **74**, 3005 (1999).
[65] R. A. Guyer and J. A. Krumhansl, Phys. Rev. **148**, 766 (1966).
[66] G. Chen and C. L. Tien, J. Thermophys. Heat Transfer **7**, 311 (1993).
[67] G. Chen, S. Q. Zhou, D.-Y. Yao, C. J. Kim, X. Y. Zheng, Z. L. Liu, and K. L. Wang, in *Proceedings from 17th International Conference on Thermoelectrics* (IEEE, Piscataway, NJ, 1998), pp. 202–205.
[68] C. Moglestue, Comput. Methods Appl. Mech. Eng. **30**, 173 (1982).
[69] C. Jacoboni and L. Reggiani, Rev. Mod. Phys. **55**, 642 (1983).
[70] P. Lugli, P. Bordone, L. Reggiani, M. Reiger, P. Kocevar, and S. M. Goodnick, Phys. Rev. B **39**, 7852 (1989).
[71] M. V. Fischetti and S. E. Laux, Phys. Rev. B **38**, 9721 (1988).
[72] M. V. Fischetti and S. E. Laux, Phys. Rev. B **48**, 2244 (1993).
[73] T. Klistner, J. E. VanCleve, H. E. Fischer, and R. O. Pohl, Phys. Rev. B **38**, 7576 (1988).
[74] R. B. Peterson, J. Heat Transfer **116**, 815 (1994).
[75] S. Mazumder and A. Majumdar, J. Heat Transfer **123**, 749 (2001).
[76] M. G. Holland, Phys. Rev. **134**, A471 (1964).
[77] J. Lai and A. Majumdar, J. Appl. Phys. **79**, 7353 (1996).
[78] G. D. Mahan, J. Appl. Phys. **58**, 2242 (1985).
[79] G. Chen, J. Heat Transfer **118**, 539 (1996).
[80] P. G. Sverdrup, Y. S. Ju, and K. E. Goodson, J. Heat Transfer **123**, 130 (2001).
[81] P. G. Sverdrup, S. Sinha, M. Asheghi, U. Srinivasan, and K. E. Goodson, Appl. Phys. Lett. **78**, 3331 (2001).
[82] K. Seeger, *Semiconductor Physics, Springer Series in Solid State Sciences* (Springer, Berlin, 1985), Vol. 40, p. 198.
[83] D. D. Kim and P. Y. Yu, Phys. Rev. Lett. **64**, 946 (1990).
[84] B. Jusserand and M. Cardona, in *Light Scattering in Solids V, Topics in Applied Physics*, edited by M. Cardona and G. Güntherodt (Springer, Heidelberg, 1989), Vol. 66, p. 49.
[85] O. Madelung, *Introduction to Solid State Theory* (Springer, Berlin, 1978), p. 314.
[86] K. Mizoguchi, M. Hase, S. Nakashima, and M. Nakayama, Phys. Rev. B **60**, 8262 (1999).
[87] P. Bhattacharya, *Semiconductor Optoelectronic Devices* (Prentice-Hall, Upper Saddle River, NJ, 1997).
[88] J. Urayama, T. B. Norris, J. Singh, and P. Bhattacharya, Phys. Rev. Lett. **86**, 4930 (2001).
[89] K. Schwab, E. A. Henricskon, J. M. Worlock, and M. L. Roukes, Nature (London) **404**, 974 (2000).
[90] S. Berber, Y.-K. Kwon, and D. Tomanek, Phys. Rev. Lett. **84**, 4613 (2000).
[91] M. A. Osman and D. Srivastava, Nanotechnology **12**, 21 (2001).
[92] L. D. Hicks and M. S. Dresselhaus, Phys. Rev. B **47**, 16631 (1993).
[93] J. Hone, M. Whitney, C. Piskoti, and A. Zettl, Phys. Rev. B **59**, R2514 (1999).
[94] P. Kim, L. Shi, A. Majumdar, and P. L. McEuen, Phys. Rev. Lett. **87**, 215502 (2001).
[95] J. Heremans and C. P. Beetz, Jr., Phys. Rev. B **32**, 1981 (1985).
[96] S. Volz and D. Lemonnier, Phys. Low-Dimens. Semicond. Struct. **5–6**, 91 (2000).
[97] J. Zou and A. Balandin, J. Appl. Phys. **89**, 2932 (2001).
[98] M. Doi and S. F. Edwards, *The Theory of Polymer Dynamics* (Oxford, New York, 1986).
[99] F. P. Wyart and P. G. de Gennes, Phys. Low-Dimens. Semicond. Struct. **1**, 93 (2000).
[100] K. Kurabayashi and K. E. Goodson, J. Appl. Phys. **86**, 1925 (1999).
[101] International Technology Roadmap for Semiconductors, 1998 Update (Semiconductor Industry Association, San Jose, CA, 1999).
[102] Y. L. Shen, J. Vac. Sci. Technol. B **17**, 2115 (1999).
[103] B. C. Daly, G. A. Antonelli, H. J. Maris, W. K. Ford, L. Wong, and E. Andideh, Physica B **316–317**, 254 (2002).
[104] W. S. Capinski and H. J. Maris, Rev. Sci. Instrum. **67**, 2720 (1996).
[105] E. B. Varner, T. Marieb, A. S. Mack, J. Lee, W. K. Meyer, and K. E. Goodson, Mater. Res. Soc. Symp. Proc. **473**, 279 (1997).
[106] A. Grill and V. J. Patel, J. Appl. Phys. **85**, 3314 (1999).
[107] B. K. Hwang, M. J. Loboda, G. A. Cerny, R. F. Schneider, J. A. Seifferly, and T. Washer, *Proceedings of the IEEE 2000 International Interconnect Technology Conference* (IEEE, Piscataway, NJ, 2000), pp. 52–54.
[108] D. G. Cahill, S. K. Watson, and R. O. Pohl, Phys. Rev. B **46**, 6131 (1992).
[109] C. Hu, M. Morgen, P. S. Ho, A. Jain, W. N. Gill, J. L. Plawsky, and P. C. Wayner, Appl. Phys. Lett. **77**, 145 (2000).
[110] R. M. Costescu, A. J. Bullen, G. Matamis, K. E. O'Hara, and D. G. Cahill, Phys. Rev. B **56**, 094205 (2002).
[111] D. G. Cahill, M. Katiyar, and J. R. Abelson, Phys. Rev. B **50**, 6077 (1994).
[112] R. Landauer, in *Electrical Transport and Optical Properties of Inhomogeneous Media*, edited by J. C. Garland and D. B. Tanner (American Institute of Physics, New York, 1978), pp. 2–43.
[113] J. G. Berryman, J. Acoust. Soc. Am. **91**, 551 (1992).
[114] T. Borca-Tasciuc, A. R. Kumar, and G. Chen, Rev. Sci. Instrum. **72**, 2139 (2001).
[115] K. An, K. S. Ravichandran, R. E. Dutton, and S. L. Semiatin, J. Am. Ceram. Soc. **82**, 399 (1999).
[116] D. G. Cahill and S.-M. Lee, Microscale Thermophys. Eng. **1**, 47 (1997).

[117] S.-M. Lee, G. Matamis, D. G. Cahill, and W. P. Allen, Microscale Thermophys. Eng. **2**, 31 (1998).
[118] G. Soyez, J. A. Eastman, L. J. Thompson, G.-R. Bai, P. M. Baldo, A. W. McCormick, R. J. DiMelfi, A. A. Elmustafa, M. F. Tambwe, and D. S. Stone, Appl. Phys. Lett. **77**, 1155 (2000).
[119] V. Narayanamurti, H. L. Störmer, M. A. Chin, A. C. Gossard, and W. Wiegmann, Phys. Rev. Lett. **43**, 2012 (1979).
[120] M. V. Simkin and G. D. Mahan, Phys. Rev. Lett. **84**, 927 (2000).
[121] S. Y. Ren and J. D. Dow, Phys. Rev. B **25**, 3750 (1982).
[122] S.-M. Lee, D. G. Cahill, and R. Venkatasubramanian, Appl. Phys. Lett. **70**, 2957 (1997).
[123] T. Borca-Tasciuc, W. Liu, J. Liu, T. Zeng, D. W. Song, C. D. Moore, G. Chen, K. L. Wang, M. Goorsky, T. Redetic, R. Gronsky, T. Koga, and M. S. Dresselhaus, Superlattices Microstruct. **28**, 199 (2000).
[124] T. Yao, Appl. Phys. Lett. **51**, 1798 (1987).
[125] X. Y. Yu, G. Chen, A. Verma, and J. S. Smith, Appl. Phys. Lett. **67**, 3554 (1995).
[126] W. S. Capinski, H. J. Maris, M. Cardona, D. S. Katzer, K. Ploog, and T. Ruf, Physica **263–264**, 530 (1999).
[127] S. T. Huxtable, A. R. Abramson, A. Majumdar, C. L. Tien, C. LaBounty, X. Fan, G. Zeng, J. E. Bowers, A. Shakouri, and E. T. Croke, in *Proceedings of the ASME IMECE* (ASME, New York, 2001).
[128] T. Borca-Tasciuc, D. Achimov, W. L. Liu, G. Chen, H.-W. Ren, C.-H. Lin, and S. S. Pei, Microscale Thermophys. Eng. **5**, 225 (2001).
[129] M. A. Afromowitz, J. Appl. Phys. **44**, 1292 (1973).
[130] G. Mahan, B. Sales, and J. Sharp, Phys. Today **50**, 42 (1997).
[131] R. Venkatasubramanian, Phys. Rev. B **61**, 3091 (2000).
[132] M. N. Touzelbaev, P. Zhou, R. Venkatasubramanian, and K. E. Goodson, J. Appl. Phys. **90**, 763 (2001).
[133] W. S. Capinski, H. J. Maris, T. Ruf, M. Cardona, K. Ploog, and D. S. Katzer, Phys. Rev. B **59**, 8105 (1999).
[134] S. T. Huxtable, A. R. Abramson, A. Majumdar, C. L. Tien, C. LaBounty, X. Fan, G. Zeng, J. E. Bowers, A. Shakouri, and E. T. Croke (unpublished).
[135] S. T. Huxtable, A. R. Abramson, A. Majumdar, C. L. Tien, P. Abraham, C. LaBounty, X. Fan, Y.-J. Chen, J. E. Bowers, and A. Shakouri (unpublished).
[136] P. Hyldgaard and G. D. Mahan, Phys. Rev. B **56**, 10754 (1997).
[137] G. Chen and M. Neagu, Appl. Phys. Lett. **71**, 2761 (1997).
[138] G. Chen, Phys. Rev. B **57**, 14958 (1998).
[139] G. Chen, T. Borca-Tasciuc, B. Yang, D. Song, W. Liu, T. Zeng, and D. Achimov, Therm. Sci. Eng. **7**, 43 (1999).
[140] S. Tamura, Y. Tanaka, and H. J. Maris, Phys. Rev. B **60**, 2627 (1999).
[141] G. Chen, J. Heat Transfer **121**, 945 (1999).
[142] W. E. Bies, R. J. Radtke, and H. Ehrenreich, J. Appl. Phys. **88**, 1498 (2000).
[143] A. A. Kiselev, K. W. Kim, and M. A. Stroscio, Phys. Rev. B **62**, 6896 (2000).
[144] B. Yang and G. Chen, Phys. Low-Dimens. Structures **5–6**, 37 (2000).
[145] S. Volz, J. B. Saulnier, G. Chen, and P. Beauchamp, Microelectron. J. **9–10**, 815 (2000).
[146] M. Bartkowiak and G. D. Mahan, in *Semiconductors and Semimetals* (Academic, New York, 2001), Chap. 8.
[147] A. Khitun, A. Balandin, J. L. Liu, and K. L. Wang, J. Appl. Phys. **88**, 696 (2000).
[148] A. R. Abramson, C. L. Tien, and A. Majumdar, J. Heat Transfer **124**, 963 (2002).
[149] B. C. Daly and H. J. Maris, Physica B **316–317**, 247 (2002).
[150] P. Hyldgaard and G. D. Mahan, in *Thermal Conductivity* (Technomic, Lancaster, PA, 1996), p. 172.
[151] H. Kato, S. Tamura, and H. J. Maris, Phys. Rev. B **53**, 7884 (1996).
[152] G. Chen, T. Zeng, T. Borca-Tasciuc, and D. Song, Mater. Sci. Eng., A **292**, 155 (2000).
[153] B. C. Daly, H. J. Maris, S. Tamura, and K. Imamura (unpublished).
[154] A. Asenov, R. Balasubramaniam, A. R. Brown, J. H. Davies, and S. Saini, IEDM Tech. Dig. **2000**, 279 (2000).
[155] D. A. Young, C. Thomsen, H. T. Grahn, H. J. Maris, and J. Tauc, in *Phonon Scattering in Condensed Matter*, edited by A. C. Anderson and J. P. Wolfe (Springer, Berlin, 1986), p. 49.
[156] C. A. Paddock and G. L. Eesley, J. Appl. Phys. **60**, 285 (1986).
[157] O. W. Käding, H. Skurk, and K. E. Goodson, Appl. Phys. Lett. **65**, 1629 (1994).
[158] B. M. Clemens, G. L. Eesley, and C. A. Paddock, Phys. Rev. B **37**, 1085 (1988).
[159] N. Taketoshi, T. Baba, and A. Ono, Jpn. J. Appl. Phys., Part 2 **38**, L1268 (1999).
[160] L. Shi, S. Plyasunov, A. Bachtold, P. L. McEuen, and A. Majumdar, Appl. Phys. Lett. **77**, 4295 (2000).
[161] C. C. Williams and H. K. Wickramasinghe, Appl. Phys. Lett. **49**, 1587 (1986).
[162] A. Majumdar, Annu. Rev. Mater. Sci. **29**, 505 (1999).
[163] G. Binnig, C. F. Quate, and Ch. Gerber, Phys. Rev. Lett. **56**, 930 (1986).
[164] K. Luo, R. W. Herrick, A. Majumdar, and P. Petroff, Appl. Phys. Lett. **71**, 1604 (1997).
[165] A. Hammiche, D. J. Hourston, H. M. Pollock, M. Reading, and M. Song, J. Vac. Sci. Technol. B **14**, 1486 (1996).
[166] L. Shi, O. Kwon, A. Miner, and A. Majumdar, J. Microelectromech. Syst. **10**, 370 (2001).
[167] L. Shi and A. Majumdar, J. Heat Transfer **124**, 329 (2002).
[168] L. D. Bell and W. J. Kaiser, Annu. Rev. Mater. Sci. **26**, 189 (1996).
[169] G. O. Smith, T. Juhasz, W. E. Bron, and Y. B. Levinson, Phys. Rev. Lett. **68**, 2366 (1992).
[170] R. Merlin, Solid State Commun. **102**, 207 (1997).
[171] D. J. Dieleman, A. F. Koenderink, M. G. A. Van Veghel, A. F. M. Arts, and H. W. de Wijn, Phys. Rev. B **64**, 174304 (2001).
[172] J. J. Baumberg, D. A. Williams, and K. Köhler, Phys. Rev. Lett. **78**, 3358 (1997).
[173] H.-Y. Hao and H. J. Maris, Phys. Rev. Lett. **84**, 5556 (2000).
[174] A. Macovski, *Medical Imaging Systems* (Prentice Hall, Englewood Cliffs, NJ, 1983).